Aeolian Research 77 (2026) 101070



Contents lists available at ScienceDirect

Aeolian Research

journal homepage: www.elsevier.com/locate/aeolia



Inter- and intra-annual variations in Saharan dust fluxes in the eastern Mediterranean Sea and their connection to carbon export

Anouk P.E. van Boxtel [a,b,*], Addison Rice [b,1], Constantijn Kurpershoek [b], Tijno de Nooij [b], Gert J. de Lange [b], Francien Peterse [b], Jan-Berend W. Stuut [a,c]

[a] NIOZ - Royal Netherlands Institute for Sea Research, Department of Ocean Systems, P.O.59 1790 AB Den Burg, Texel, the Netherlands
[b] UU - Utrecht University, Department of Earth Sciences, P.O. 80.115 3508, TC, Utrecht, the Netherlands
[c] VU - Vrije Universiteit Amsterdam, Department of Earth Sciences, De Boelelaan 1085 1081, HV, Amsterdam, Netherlands

ARTICLE INFO

Dataset link: Sediment-trap bulk fluxes, dust properties, and grain-size distributions at Bannock Basin, Ionian Sea (Original data)

Keywords:
Mineral dust
Sediment trap
Eastern Mediterranean Sea
Biological pump

ABSTRACT

Dust deposition in the ocean can enhance carbon export through fertilization and ballasting. However, the processes that subsequently drive the transfer of dust particles through the water column to the ocean floor remain unresolved. To assess the occurrence of vertical dust export and potential facilitating conditions we present dust fluxes and grain-size distributions collected by sediment traps in Bannock Basin, Mediterranean Sea, complemented with three years of particulate organic (POC) and inorganic (PIC) carbon fluxes. Sediment traps were deployed at three water depths (~550–800 m, ~1750–2000 m, and ~ 3000 m) for nine years between 1999 and 2011 with 10–23 days sampling intervals.

Maximum dust and total mass flux (TMF) usually occurred in spring and summer, concomitant with the season of largest atmospheric dust transport indicated by remote sensing observations. Peaks in dust fluxes occur synchronously in the three sediment traps, indicating high sinking velocities during dust events. However, not all dust events in the upper trap are transferred to the deeper traps, and average modal grain sizes are larger in the deeper traps. Furthermore, Stokesian settling velocities, corresponding to particle sizes of the dust, are too low to account for these high sinking velocities. This, combined with concomitant peaks of dust, POC, and TMF, suggests that deposited dust is mainly exported as dust-ballasted aggregates during spring and summer. However, a shift in the timing of dust flux maxima from summer to winter in 2009 suggests that the processes driving dust export may vary interannually, and emphasizes the importance of longer time series.

1. Introduction

Mineral dust deposited in the ocean has been shown to play an important role in driving the biological pump in oligotrophic oceans (e.g., Pabortsava et al., 2017). Dust fertilization can lead to increased phytoplankton productivity in low nutrient low chlorophyll regions by providing nutrients to the surface ocean (e.g., Guieu et al., 2014). However, increased primary production does not automatically lead to enhanced carbon sequestration as primary production as such does not necessarily lead to particulate organic carbon (POC) export. Instead, the efficiency of the biological pump is mainly determined by sinking velocities of POC in organic aggregates, and the remineralization of POC during settling (De La Rocha and Passow, 2007; Guerreiro et al., 2021). Hence, rapid POC export after dust-related primary production is essential for potential CO_2 sequestration.

The close relationship between POC and mineral fluxes in the deep ocean suggests that POC export in oligotrophic regions depends on mineral ballasting that increases the sinking velocity of settling POC (Armstrong et al., 2002; Francois et al., 2002; Klaas and Archer, 2002). Ballast minerals can be of biogenic origin, i.e., in-situ produced $CaCO_3$ or opal, or of lithogenic origin, e.g., aeolian mineral dust. Hence, dust deposition can also contribute to vertical export of POC through ballasting effects in addition to its fertilizing effects (e.g., Pabortsava et al., 2017).

Roller tank experiments have shown that incorporation of ballast minerals, including mineral dust, can indeed increase sinking velocities of POC by increasing excess density of organic aggregates, i.e., marine snow and zooplankton fecal pellets (Ploug et al., 2008a; Ploug et al.,

* Corresponding author at: NIOZ - Royal Netherlands Institute for Sea Research, Department of Ocean Systems, P.O.59 1790 AB Den Burg, Texel, the Netherlands.
E-mail address: anouk.van.boxtel@nioz.nl (A.P.E. van Boxtel).
[1] ETH Zürich, Department of Earth Sciences, NO D 63, Sonneggstrasse 58,092 Zürich, Switzerland

https://doi.org/10.1016/j.aeolia.2026.101070
Received 5 December 2025; Received in revised form 6 May 2026; Accepted 6 July 2026
Available online 10 July 2026
1875-9637/© 2026 Published by Elsevier B.V.

2008b; Iversen and Robert, 2015). Additionally, deposited dust can also trigger aggregate formation by acting as aggregation nuclei, further increasing settling rates (Iversen and Robert, 2015; Van der Jagt et al., 2018), or by triggering the formation of sticky transparent exopolymer particles (TEP) that also induce aggregate formation (Louis et al., 2017). However, increased sinking velocities also result in increased oxygen fluxes to sedimenting aggregates, which can lead to increased degradation rates (Ploug et al., 2008a). Additionally, contact between organic aggregates and ballast minerals has been shown to result in disaggregation or size reduction of aggregates (Passow et al., 2014; Iversen and Robert, 2015), reducing settling velocities. Nevertheless, increased settling velocities due to ballasting overall seems to outweigh the effects of increased degradation rates and aggregate disaggregation on vertical POC export efficiency (Iversen, 2023).

The Mediterranean Sea is an ultra-oligotrophic basin where ballasting by dust might play an important role in driving organic carbon export due to its proximity to the Sahara Desert, and resulting high dust input, in combination with low primary production. Indeed, several sediment-trap studies in the Mediterranean Sea show a relationship between POC and dust export, both in the Western Mediterranean Sea (WMS; e.g., Migon et al., 2002; Lee et al., 2009; Ternon et al., 2010) and the Eastern Mediterranean Sea (EMS; e.g., Patara et al., 2009; Stavrakakis et al., 2013; Tsagkaraki et al., 2020; Pedrosa-Pamies et al., 2021; Van Boxtel et al., 2025). However, not all atmospheric dust events are associated with increased carbon export, and deposited dust is not always directly exported to the deep ocean. For example, a large dust event in the WMS in 2004 resulted in an increase in primary production followed by POC export captured by sediment traps, but dust deposited during other events was not captured by the traps (Ternon et al., 2010). Instead, this dust likely remained trapped in the surface ocean until it was transported by another mechanism, such as convective mixing or zooplankton activity (Migon et al., 2002; Ternon et al., 2010). In the Cretan Sea, seven years of sediment-trap dust and POC fluxes showed that dust deposition in spring appears to have a stronger effect on total particle export, i.e., export of both biogenic and lithogenic material, compared to dust deposition in fall (Theodosi et al., 2019). This difference was attributed to higher primary productivity and, therefore, POC availability for aggregate formation in spring compared to in fall, suggesting that POC availability drives dust export instead of the other way around (Tsagkaraki et al., 2020). Sediment traps in the central Ionian Sea also registered increased dust and POC export during spring in two consecutive years, although the increase in POC export varied substantially between the two years. The interannual difference in POC export was attributed to differences in modal particle size of the dust fraction, which may in turn have been associated with different dust transport pathways (Van Boxtel et al., 2025). Hence, the exact dynamics of dust export and its relationship with POC availability and export seem to vary seasonally and interannually, but the mechanisms driving dust-associated POC export remain understudied. Moreover, nutrient concentrations and the degree of vertical mixing in the Mediterranean Sea decrease towards the east, resulting in spatial differences in the amount and timing of primary production, which likely induces spatial variation in the relationship between dust and POC export.

To assess (1) when deposited dust is transferred through the water column; (2) what conditions facilitate the export of deposited dust; and (3) what the implications of these mechanisms and conditions are for ballasting effects of dust in the EMS, we studied a long-term (nine years of sampling between 1999 and 2011) high-resolution (10–23 day sample intervals) time series of dust fluxes and total mass fluxes (TMFs) in Bannock Basin, Ionian Sea, EMS. Sediment traps were moored at three different water depths (~550–800 m, ~1750–2000 m and ~3000 m), which allows for estimating sinking rates. We use the grain-size distributions of the dust deposited in the sediment traps to study how dust particles settle in the ocean after deposition by comparing Stokesian sinking velocities of individual dust particles calculated from their modal grain size to minimum sinking velocities of dust particles based on the timing of peaks in dust fluxes at different sediment traps and the depth difference between the traps. Additionally, we assess the potential use of grain-size distributions in the sediment traps as a proxy for (seasonal) differences in dust transport pathways or deposition modes. Additionally, we have analyzed three years of POC and particulate inorganic carbon (PIC) fluxes in the same material to evaluate the relationships between dust and carbon export. To assess the effects of (seasonal) variations in oceanographic and atmospheric conditions on the export of dust and carbon, we have compared the sediment-trap records to remote-sensing and reanalysis-based time series of aerosol optical depth (AOD), precipitation, sea surface temperature (SST), mixed layer depth (MLD) and chlorophyll *a* (Chl*a*) concentration in the surface ocean.

2. Oceanographic and atmospheric setting

The EMS is characterized by an anti-estuarine circulation pattern: nutrient-depleted surface waters flow into the Mediterranean Sea through the strait of Gibraltar and become progressively more oligotrophic flowing east, while deeper water enriched in nutrients flows out into the north Atlantic Ocean, resulting in a net loss of nutrients (Krom et al., 2003). Surface circulation in the EMS consists of Modified Atlantic Water (MAW) that enters the EMS through the strait of Sicily where it forms a large cyclonic loop, sub-basin scale (semi)permanent gyres, and wind or instability-induced eddies. The surface circulation in the south Ionian Sea is mainly affected by the Atlantic Ionian Stream (AIS) and the Syrte Gyre (Pinardi et al., 2015). Additionally, the Ionian Sea surface circulation also varies seasonally: in winter, the circulation mainly consists of relatively stable veins, while in summer, the circulation is less stable and trains of mainly anticyclonic eddies can form, particularly in the south Ionian Sea (Estournel et al., 2021). These mesoscale features result in a large spatial heterogeneity in e.g., nutrient concentrations, thereby affecting primary productivity, phytoplankton community composition, and blooming regimes (Casotti et al., 2003; Siokou-Frangou et al., 2010; Varkitzi et al., 2020). Particularly during spring, the simultaneous occurrence of multiple surface water masses results in a patchwork of blooming and non-blooming areas (Casotti et al., 2003; Berline et al., 2021). In addition to seasonal variability, the Ionian Sea circulation is affected to a great extent by decadal reversals of the direction of the northern Ionian Gyre as a result of the bimodal oscillating system (BiOS), which affects the distribution of water masses in the EMS (Gačić et al., 2010; Civitarese et al., 2023). The BiOS-related changes in surface circulation also affect nutrient concentrations, primary production, and phytoplankton phenology in the Ionian Sea (Civitarese et al., 2010; Lavigne et al., 2018; Civitarese et al., 2023).

The main vertical water masses in the Ionian Sea consist of MAW (0–200 m), Levantine Intermediate Water (LIW) that is formed in the Levantine Sea and flows westward to the Ionian Sea (~200–600 m; Skliris, 2014), and Eastern Mediterranean Deep Water (EMDW; >1200 m) that is formed in the Adriatic or Aegean Sea by deep convection, or the Cretan Sea (Fig. 1; Poulos, 2023, and references therein; Schroeder et al., 2024). The two deeper traps in this study were located in the EMDW throughout the study period (Fig. 1). However, the upper trap is located around the lower boundary of the LIW layer. Furthermore, an extra intermediate water layer, the Transitional Mediterranean Water (TMW) which consist of mixed LIW and EMDW, occurs occasionally at 400–800/1200 m (Poulos, 2023, and references therein; Schroeder et al., 2024). Furthermore, the water mass structure in the Ionian Sea is characterized by a strong interannual variability (Gačić et al., 2011). This implies that the upper trap could have been located in the LIW or TMW or even the EMDW, depending on the exact mooring depth and prevailing conditions.

Nutrient concentrations and primary production in the EMS are low year-round, although they vary seasonally due to differences in water column mixing throughout the year. The EMS is stratified continuously from May to October (D'Ortenzio et al., 2005). Correspondingly, surface

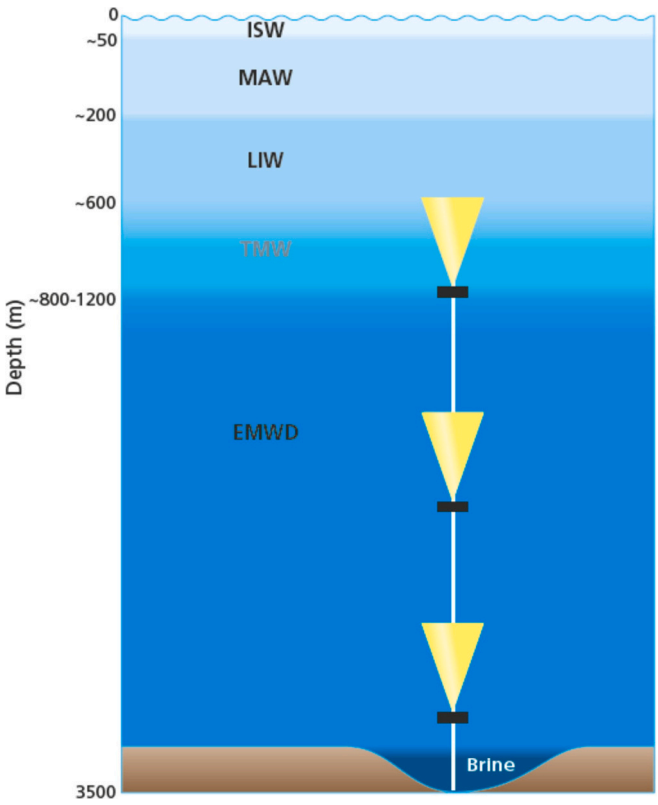


Fig. 1. Vertical distribution of the water masses in the Ionian Sea surrounding the sediment traps. Permanent water masses are indicated in black text; non-permanent water masses are indicated in grey text. ISW: Ionian Surface Water; MAW: Modified Atlantic Water; LIW: Levantine Intermediate Water; TMF: Transitional Mediterranean Water; EMDW: Eastern Mediterranean Deep Water. After Skliris (2014), Poulos (2023), and Schroeder et al. (2024).

Chl*a* concentrations are lowest during summer as stratification prevents mixing of deeper, more nutrient-rich water. During winter, surface-ocean cooling and winter storms result in enhanced mixing, bringing deeper, nutrient-enriched waters to the surface ocean, resulting in increased surface Chl*a* concentrations (Krom et al., 2003). However, as the mixing depth during winter in the EMS usually does not reach the nutricline, nutrient concentrations and primary production in the EMS also remain relatively low during winter compared to other oligotrophic basins including the WMS. Additionally, a well-established deep chlorophyll maximum occurs year-round and primary production also occurs deeper in the water column, particularly during summer stratification (Boldrin et al., 2002; Casotti et al., 2003; Krom et al., 2003; Marañón et al., 2021).

Dust transported over the EMS is mainly derived from the nearby North African deserts (Guerzoni et al., 1999; Stuut et al., 2009). Dust sources mainly consist of playas and dried-up lake beds (Prospero et al., 2002; Tegen et al., 2002), although dust may also be derived from sand dunes (Crouvi et al., 2012). Although the atmosphere above north Africa is almost permanently loaded with dust, dust transport to the Mediterranean Sea only occurs during synoptic events when depressions generate northward winds that deviate from the typical north-west wind direction over the Mediterranean (Moulin et al., 1998; Israelevich et al., 2002).

Dust transport pathways to the Mediterranean Sea vary seasonally (Moulin et al., 1998; Israelevich et al., 2002; Israelevich et al., 2012; Varga et al., 2014): generally, dust is mostly transported over the WMS towards the EMS during spring, and gradually penetrates less far east during summer (Israelevich et al., 2002). Dust transport to the Ionian Basin has a bimodal shape with peaks in spring and summer (Israelevich et al., 2012; Varga et al., 2014). As different synoptic meteorological situations drive these two transport routes, main dust sources vary throughout the year. Overall, dust transported to the central and eastern Mediterranean during early spring is mainly derived from the Libyan deserts, while in June, most dust is sourced from northwestern Africa (Moulin et al., 1998).

Due to the ultraoligotrophic conditions and lack of new nutrient supply from deeper water masses, atmospheric dust deposition is a major source of new nitrogen and phosphate in the EMS (Krom et al., 2004). Particularly, dust deposited during summer, when surface waters are depleted in nutrients due to stratified conditions, could be fueling primary production. In summary, a complex interplay of a large set of atmospheric and oceanographic features may determine whether dust deposition leads to a phytoplankton response, and if dust deposition leads to enhanced carbon export to the deep Mediterranean Sea.

3. Material & Methods

3.1. Sample collection and processing

Sinking particles were collected in Technicap PPS5/2 sediment traps (diameter 1 m^2) in the 3500 m deep Bannock Basin in the south Ionian Sea (34.37°N, 20.01°E). In total, nine sediment-trap moorings were deployed from 1999 to 2011 (10–23-day resolution), including several smaller gaps and one larger hiatus from fall 2006 to fall 2008. In general, sediment traps were deployed at two or three water depths corresponding to three general categories: “upper” (545–800 m), “middle” (1750–2030 m), and “lower” (2955–3120 m). During some deployments, the upper and some of the middle trap collection bottles were poisoned with formalin to prevent microbial degradation of organic material. For the middle trap no systematic differences were observed between poisoned and unpoisoned samples. An overview of the exact mooring conditions and sample treatment of all deployments is given in Table S1. After retrieval, samples were split on-board into eight aliquots and filtered onto glass fiber filters (GF/F; $n = 3$) and cellulose acetate filters (pore size 0.2 µm, $n = 4$) which were not pre-weighed. After splitting, samples were either stored at 4 °C or -18 °C (Table S1). Before analysis, samples were freeze-dried.

3.2. Sediment-trap sample analysis

3.2.1. Total mass fluxes

To determine TMF, two freeze-dried 1/8th aliquots on GF/Fs were weighed. As the GF/F filters were not preweighed, the average empty GF/F filter weight was estimated. First, for 210 samples, an aliquot on an oven-dried cellulose acetate filter was weighed, sediment-trap material was removed with water, and the empty oven-dried filter was weighed again to determine the mass of the aliquot itself. Next, the weight of the aliquot from the cellulose acetate filter was compared with the weight of the three aliquots on the GF/Fs to determine the average weight of the GF/F filters. This was then used to correct the weight from all aliquots on GF/Fs for filter mass. TMF was determined from two aliquots to reduce the uncertainty from the variability in GF/F weight and between aliquots of a given sample. TMFs for the lower trap for the PS80 and BP01 deployments have been published in Patara et al. (2009).

3.2.2. Lithogenic fluxes and grain-size distributions

Lithogenic fluxes and grain-size distributions were analyzed for all deployments. To isolate the lithogenic fraction, all biogenic material was removed. First, one 1/8th aliquot on cellulose acetate filters of each sample was ashed in a low temperature plasma asher for 7–24 h to isolate the filtrate from the cellulose acetate filter, also removing all organic material in the filtrate. For the deeper traps, this was sufficient to remove all organic material, but for some of the upper trap samples organic matter content was too high for complete removal of organic material after 24 h. To ensure complete removal of organic material in the upper trap samples as well, excess (2–5 ml) H_2O_2 (35%) was added

in ~20 ml reversed osmosis (RO) water and boiled until all H_2O_2 had reacted or decomposed into H_2O and O_2. Next, biogenic carbonate and silica were chemically removed following McGregor et al. (2009). In brief, samples were boiled in 25 ml RO water with excess (2 ml) HCl (10%) for exactly 1 min to remove biogenic carbonates. Next, samples were boiled for 10 min with 2 g of NaOH pellets in 25 ml RO water to remove biogenic silica. After both the carbonate and silica removal steps, samples were neutralized twice by adding RO water to a volume of 250 ml, allowing the particles to settle for a minimum of 7 h, and decanting to 25 ml.

Particle-size distributions of the lithogenic fraction were measured with a Coulter laser diffraction particle sizer (LS13 320) with a micro liquid module (MLM). Particles were suspended in degassed RO water to prevent air bubbles from altering the results and kept in suspension during analysis using a magnetic stirrer. To obtain dust masses, the lithogenic fraction was filtered over pre-weighed polycarbonate filters (25 mm, 0.2 μm pore size) and re-weighed after drying.

Non-parametric end-member analysis (EMA) with three end members was performed on the grain-size distribution dataset to unmix grain-size distributions to better assess potential differences in e.g., transport pathways or export mechanisms in the time-series. EMA was performed with the AnalySize algorithm (Paterson and Heslop, 2015) as this algorithm performs best for sediments of aeolian origin (Van Hateren et al., 2018).

3.2.3. Carbon content and fluxes

POC and PIC fluxes were analyzed for three deployments where traps were present at all three depths (PS80, BP01, and NU01). To determine POC and PIC fluxes, POC and total carbon (TC) content were analyzed using a Thermo Scientific Flash elemental analyzer (EA) at Utrecht University.

To meet the requirements for the amount of carbon per sample necessary for reliable measurements (~30 μg), subsamples were taken from 1/8th aliquots on GF/F filters. Subsamples were either taken by taking punches with a known area of the filter including sediment for homogeneously distributed, small-mass samples, or by weighing-in a small amount of homogenized sediment scraped off the filter for sufficiently large (large-mass) samples. Ideally, for consistency, one of the two approaches would be used for all samples. However, this was not possible due to large variation in the amount of sediment on the filters between samples, and because the filters were not pre-weighed before filtration on-board. For punched samples, carbon content was determined by measuring the amount of carbon on punched GF/F filters with a known surface area, correcting for the full filter area, and calculating fluxes from this. For weighed-in samples, carbon content was measured as %wt of the weighed-in samples and fluxes were obtained by multiplying %wt carbon content with calculated TMF.

Samples for POC analysis were first decalcified by acid fumigation for 16 to 24 h in a desiccator with a large petri dish filled with fuming HCl (37%) following Komada et al. (2008). Subsamples of high-mass samples and punches of low-mass samples with a punch area < 20 mm^2 were placed in the desiccator in silver sample cups; punches with a filter area > 20 mm^2 were placed in glass petri dishes to ensure contact of the complete punch with the acid fumes. Subsequently, samples in sample cups were dried on a 60 °C heating plate for three hours; punches in petri dishes were dried in a 60 °C stove for three hours after air-drying for one hour. Samples for TC, either filter punches or weighed-in sediment, were placed in tin sample cups and remained untreated.

POC and TC fluxes from punched filters were calculated as:

$$\textit{Carbon flux}\ (mg\ m^{-2}\ d^{-1}) = \textit{carbon content}_{punch}\ (mg)^{*}\left(\textit{total filter area}_{GF/F\ filter}\Big/\textit{filter area}_{punch}\right)^{*} 8 \Big/ \left(\textit{trap area}\ (m^2)^{*}\ \textit{bottle open period}\ (d)\right);$$

POC and TC fluxes from scraped samples were calculated as:

$$\textit{carbon flux} = \textit{carbon content}_{sample}\ (\%)^{*}\ \textit{TMF};$$

PIC fluxes were calculated as:

$$TC_{flux} - POC_{flux};$$

carbon content (%) of punched samples was calculated as:

$$\textit{carbon content}\ (\%) = \textit{carbon flux}/\textit{TMF}^{*}\,100.$$

No carbon content was calculated for samples with a TMF <1 mg m^{-2} d^{-2} as uncertainties for these samples are too high to yield reliable POC and PIC content.

3.3. Oceanographic and atmospheric conditions

To compare the sediment-trap time series to oceanographic and atmospheric conditions, satellite-derived and reanalysis-based time series of atmospheric and oceanographic parameters were retrieved. Atmospheric parameters included area-averaged monthly and daily AOD at 550 nm (unitless) and daily precipitation (mm d^{-1}) and were retrieved from the NASA Giovanni online data system for a $1 \times 1°$ grid box around the sediment trap; oceanographic parameters included daily SST (°C) and MLD (m) and monthly Chl*a* concentration (mg m^{-3}) and were retrieved for the sediment trap site from the Copernicus Marine Service Information (CMEMS). Further details can be found in Table S2.

As AOD at 550 nm is a measure of atmospheric aerosol load, it is here used to assess atmospheric dust transport over the sediment-trap site. However, AOD also registers aerosols from soot and volcanic ash. Hence, potential dust events registered in the AOD record were also visually compared to satellite images of the sediment-trap region in NASA Worldview.

3.4. Data handling

Some samples were excluded from the data set. One sediment trap got stuck during deployment. As a result, some bottles got stuck under the funnel and collected material for a longer time period, leaving the following bottles that did not rotate under the funnel empty. Hence, these samples were excluded from further analysis. Additionally, during some deployments, the last bottle was still located under the funnel upon retrieval. As these bottles contain abnormally large amounts of sediment, they likely also contain sediments from the water column and potentially also sediment that got stuck on the funnel surface during the mooring period (Rutten et al., 2000; Malinverno et al., 2014). Hence, these samples were also excluded. Additionally, two filters from the upper trap that contained rotting fish remains were excluded from analysis.

Average fluxes were calculated over the entire interval, taking the variable bottle-open period into account (e.g., with a similar flux, a 10-day sample holds half the weight of a 20-day sample). Flux-weighted averages of lithogenic, POC, and PIC content as well as modal grain size were also calculated while accounting for sample duration.

Additionally, cross correlations between the sediment-trap parameters as well as the correlation of parameters between different trap depths were calculated using the cross-correlation function in base R. Cross correlations were calculated for each deployment separately due to unreconcilable differences in sampling resolution and time gaps

between deployments. Smaller gaps within the deployments (max. two bottles, except for one three-bottle gap in the middle trap of the NU01 deployment) were linearly interpolated.

4. Results

4.1. Bulk fluxes

4.1.1. Total mass flux (TMF)

Between September 1999 and January 2011, the TMF ranged from 0–209.6, 0–172.6, and 0–122.8 mg m^{-2} d^{-1}, in the upper, middle, and deepest trap, respectively (Fig. 2; Table 1). Over the complete study period, the daily average TMF in the upper trap was more than twofold larger than in the two deeper traps (46.4, 16.2 and 15.6 mg m^{-2} d^{-1} for the upper, middle, and lower traps respectively; Table 1). Overall, TMF was slightly higher in the middle trap compared to the lower trap, although in 2002 and the first half of 2010, fluxes in the deepest trap were substantially larger, resulting in the comparable annually averaged TMF (Fig. 2; Table 1).

TMF in the upper trap was generally low in fall and winter and peaked one or two times per year in spring and summer from 1999 to 2005, although the exact timing and magnitude of the TMF maxima varied substantially between years (Fig. 2). In addition to these large increases in TMF in spring and/or summer, smaller increases in TMF were observed occasionally in winter and fall (Fig. 2). In 2009 and 2010, after the sampling hiatus (2006–2008), large TMFs also occurred in spring and summer, although the major TMF peak occurred in winter during these years. Furthermore, minimum TMF was larger than in the period before the hiatus, and in 2009, the flux varied much less on a seasonal basis than in other years (Fig. 2). For all depths, average TMF varied substantially between deployments (Table 2).

In the two deeper traps, sustained maxima in TMF usually occurred once every year synchronously with increased TMFs in the upper trap, except from 2005, when no clear peak in TMF was observed in the deeper traps (Fig. 2). From 1999 to 2004, annual peaks generally occurred from spring to late summer, while in 2006 the TMF peak was already observed in late winter-early spring. After the hiatus, TMF peaked in early winter 2009, and in late winter in 2010 (Fig. 2). Notably, some large TMF maxima in the upper trap were not transferred to the deeper traps, i.e., from late summer to fall 2000, and summer 2005, 2009 and 2010. Additionally, some smaller and shorter-lived peaks in TMF that were recorded in the lower traps were not represented in the upper trap, e.g., in fall 2001, 2002, and 2003, and winter 2002 and 2004.

4.1.2. Lithogenic fluxes

Lithogenic fluxes ranged from 0.1–120, 0–50.3, and 0–59.9 mg m^{-2} d^{-1} in the upper, middle, and lower trap, respectively (Fig. 2; Table 1). Peaks in lithogenic fluxes occurred mostly during spring and summer, coinciding with peaks in TMF. However, while sustained increased TMFs in the deeper traps were observed occasionally during winter, e.g., in 2002, peaks in lithogenic fluxes were restricted to spring and summer. Additionally, from 2008 to 2011, the amplitude of the lithogenic fluxes in the upper trap was more variable compared to the sustained high TMF during this interval (Fig. 2).

Similar to the TMF, lithogenic fluxes were again substantially larger in the upper trap compared to the deeper traps over the studied interval with average lithogenic fluxes over the complete study period of 10.8, 4.2 and 4.4 mg m^{-2} d^{-1} in the upper, middle, and lower trap, respectively (Table 1). Flux-weighted average lithogenic content over the complete study period increased with trap depth from 20.5% in the upper trap to 24.9% in the middle trap, and 30.7% in the deepest trap (Table 1).

4.1.3. Particulate organic and inorganic carbon fluxes

POC fluxes in the upper, middle, and lower traps ranged from 0 to 5.0, 0–2.7, and 0–2.2 mg m^{2} d^{-1}, respectively, during the three years they were analyzed (Table 1). Average POC fluxes decreased substantially between the upper and middle trap and remained similar between the middle and lower trap (1.1, 0.4 and 0.3 mg m^{-2} d^{-1}, respectively; Table 1). Flux-weighted average POC content also decreased with trap depth from 4.6%, 3.8% and 3.1% in the upper, middle and lower trap, respectively.

PIC fluxes ranged from 0 to 5.0, 0–1.9, and 0–1.5 mg m^{-2} d^{-1}, in the upper, middle, and lower trap, respectively. Similar to POC fluxes, average PIC fluxes decreased substantially between the upper and middle trap, but not between the middle and lower trap (0.7, 0.3 and 0.2 mg m^{-2} d^{-1}, respectively), and flux-weighted average PIC content decreased from 2.9% in the upper trap to 2.7% in both the middle and lower trap (Table 1).

Overall, seasonal patterns of POC and PIC fluxes were similar to TMF to the same trap, although in late summer-fall of 2000 and 2004, an additional peak in POC and PIC flux occurred without a clear corresponding peak in TMF and dust flux (Fig. 2).

4.2. Grain-size distributions

Grain sizes ranged from 0.4 μm (lower detection level) to ~170 μm (Fig. 3). Visually, two main different distribution types can be distinguished in the dataset, one relatively fine-grained and one relatively coarse-grained. The finer-grained distributions were typically characterized by a major peak with a mode ranging from ~10 to ~20 μm, and a secondary coarser peak or shoulder ranging from ~30–40 μm (Fig. 3). The coarser-grained distributions with a mode > 20 μm generally did not have a (visible) secondary coarse shoulder, although some of these samples do show a second mode at ~50 μm (Fig. 3).

To better visualize potential changes in grain size over time and with depth, variation in modal grain size of the dust, i.e., the grain-size bin with the highest frequency of the distribution, was assessed. The modal grain size is more suitable for coarse-shouldered or bimodal grain-size distributions than the mean or median (Stuut et al., 2005; Van der Does et al., 2016; Van der Does et al., 2018). Modal grain sizes ranged from 7.1 to 38.0 μm (Fig. 2; Table 1).

Overall, flux-weighted average modal grain size was slightly smaller the upper trap (13.4 μm; Table 1) compared to the deeper traps (15.5 μm in the middle trap and 14.7 μm in the lower trap). Additionally, modal grain sizes of samples from the same time interval differed substantially between trap depths, even though peaks in total particle fluxes, dust fluxes, and carbon fluxes occurred synchronously at the different water depths (Fig. 2).

4.3. Oceanographic and atmospheric background conditions

Surface ocean Chl*a* concentrations and SSTs varied seasonally in opposite phase: maximum Chl*a* and minimum SST usually occurred in late winter-early spring, while maximum SST and minimum Chl*a* concentrations usually occurred in summer (Fig. 4). MLD also varied seasonally, with maximum MLDs in winter and minimum MLDs in summer (Fig. 4). In contrast to SST and Chl*a* concentration, MLD changed less gradually, usually with a sharp decline in spring, and a more gradual increase in late summer-fall.

Daily AOD varied between < 0.01 and 3.1, where AOD values > 0.5 indicate hazy skies, or atmospheric dust events. Based on AOD, dust events occurred year-round (Fig. 4), although more often during spring-summer. Furthermore, strongest dust events with highest AOD mainly occurred in spring and summer. Notably, various gaps in the daily AOD record occurred due to cloud coverage. Monthly AOD varied seasonally with one or two maxima in spring and/or summer and minima in fall and winter, although less regular in timing compared to Chl*a* and SST (Fig. 4). From 2000 to 2005, monthly AOD had a bimodal pattern, with a first peak in spring and a second peak in summer. From 2005 to 2006, AOD varied more gradually than in the preceding interval without clear

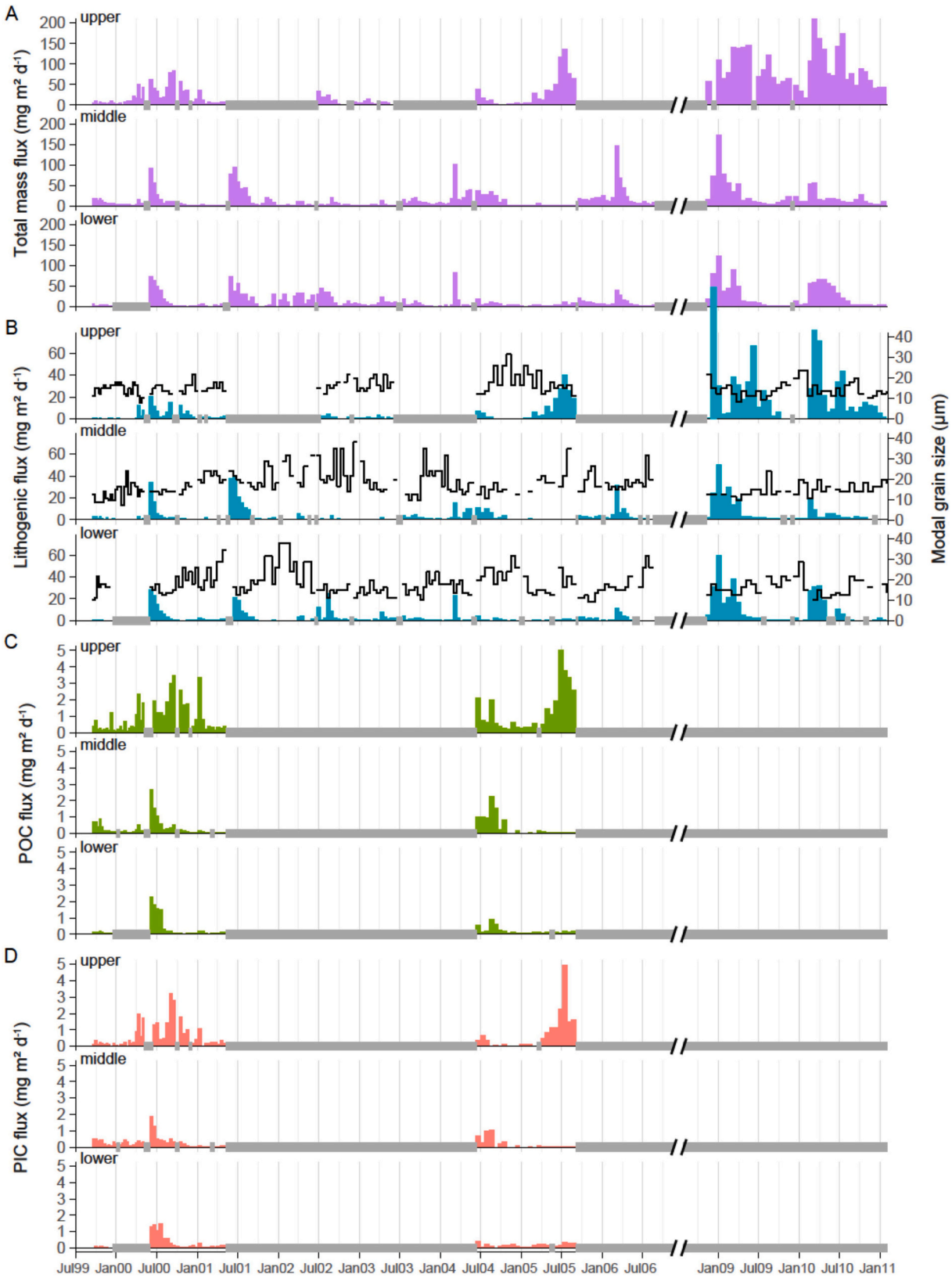


Fig. 2. Bulk fluxes in the upper, middle, and lower sediment traps: (A) Total mass flux (TMF); (B) lithogenic flux (bars) and modal grain size of the lithogenic fraction (black line); (C) particulate organic carbon (POC) flux; and (D) particulate inorganic carbon (PIC) flux. Grey bars indicate intervals without samples or measurements.

Table 1
Descriptive statistics of the total and bulk fluxes (mg m^{-2} d^{-1}), relative contribution (%), and grain size characteristics (mode and standard deviation of the grain-size distribution of the lithogenic fraction) at the different trap depths. Averages correspond to time-weighted averages for fluxes, and flux-weighted averages for the relative contributions and grain-size characteristics. Min: minimum flux; max: maximum flux; sd: standard deviation; n: amount of samples used for the calculations.

Measurement	Depth	Average	min	max	sd	n
Total mass flux	Upper	46.4	0	209.6	44.6	127
	Middle	16.2	0	172.6	23.3	199
	Lower	15.6	0	122.8	19.9	190
Lithogenic flux	Upper	10.8	0	120	17.1	128
	Middle	4.2	0	50.3	7.5	188
	Lower	4.4	0	59.9	8.2	175
Particulate organic carbon flux	Upper	1.1	0	5.0	1.1	66
	Middle	0.4	0	2.7	0.5	62
	Lower	0.3	0	2.2	0.5	55
Particulate inorganic carbon flux	Upper	0.7	0	5	0.9	64
	Middle	0.3	0	1.9	0.3	61
	Lower	0.2	0	1.5	0.3	54
% Lithogenic	Upper	20.5	0	53.0	11.1	121
	Middle	24.9	0	66.2	12.7	175
	Lower	30.7	0	79.8	17.0	168
% Particulate organic carbon	Upper	4.6	0.8	32.9	5.2	64
	Middle	3.8	0.9	12.4	1.9	55
	Lower	3.1	0.7	15	2.3	50
% Particulate inorganic carbon	Upper	2.9	0	7.3	1.6	65
	Middle	2.7	0	12.5	2.6	56
	Lower	2.7	0	12.3	2.6	50
Modal grain size	Upper	13.4	7.8	31.5	3.9	125
	Middle	15.5	7.1	38	5.7	175
	Lower	14.7	9.4	38	5.8	173
Standard deviation of grain size distribution	Upper	2.5	2.2	2.7	0.1	125
	Middle	2.5	2.1	3	0.1	175
	Lower	2.5	2.1	3	0.1	173

seasonal peaks, although minimum values still occurred in winter. From 2007 onwards, monthly AOD was again more variable between seasons, but the timing of AOD maxima varied from year to year. In 2009, largest AOD values occurred in winter, deviating from the general pattern of lowest AOD values in winter during the other years. In 2010, the daily AOD record indicated that large dust events also occurred in winter, but these dust events were not registered in the monthly record (Fig. 4).

Daily precipitation varied between 0 and 88.1 mm and was generally out-of-phase with AOD, with maximum amounts in late fall and winter and low amounts in spring and summer (Fig. 4).

5. Discussion

5.1. Particle fluxes at Bannock Basin

5.1.1. Absolute total particle fluxes and trapping efficiency

The absolute TMFs at Bannock Basin (average 46.4, 16.2, and 15.6 mg m^{-2} d^{-1} in the upper, middle, and lower trap, respectively; Table 1), are relatively low compared to other sites in the open Mediterranean Sea such as in the Cretan Sea (89.6 and 97.4 mg m d^{-1} at 500 and 1715 m; Theodosi et al., 2019), at the NESTOR site in the eastern Ionian Sea (ranging from 34 mg m^{-2} d^{-1} at 3200 m to 66 mg m^{-2} d^{-1} at 700 m; Stavrakakis et al., 2013), and in the central Ionian Sea (33.5 mg m^{-2} d^{-1} at 2340 m; Van Boxtel et al., 2025). However, the TMFs observed here are comparable to sediment-trap studies in the nearby Urania Basin (17 mg m^{-2} d^{-1} at 500 m and 13 mg m^{-2} d^{-1} at 2500 m; Malinverno et al., 2014; Patara et al., 2009) and the northern Ionian Sea (8.68 mg m^{-2} d^{-1} at 2250 m; Boldrin et al., 2002). The average TMF of the lower trap is also similar to the TMF at the same site from 1991 to 1994 (15.9 mg m^{-2} d^{-1} at 3000 m; Rutten et al., 2000).

The relatively low particle fluxes at the study site could be associated with the ultra-oligotrophic nature of the basin, even compared to the generally oligotrophic EMS. However, differences in sampling efficiency of the different types of sediment traps used in these studies (e.g., 0.125 m^2 Technicap PPS3/3, 0.5 m^2 KUM) cannot be excluded (Buesseler et al., 2007). Furthermore, Rutten et al. (2000) calculated a trapping efficiency of only 23% for the 1991–1994 interval based on Thorium-230 (^{230}Th) fluxes for the same mooring location and sediment-trap type (Technicap PPS5/2) as used for this study. Although this suggests that the particle fluxes reported here could underestimate the true particle flux, consistent use of the same sediment-trap type for all deployments allows for direct comparison of absolute fluxes in the current dataset.

Additionally, the sampling efficiency of sediment traps can be affected by lateral currents affecting interception by the traps. However, for the years where current-meter data was available, current speed was mainly below or near the detection limit, and current meters deployed with an earlier sediment-trap mooring at the same site never detected current speeds > 7 cm s^{-1} (Rutten et al., 2000) over the traps, which is substantially lower than a threshold of 15 cm s^{-1} that is generally considered as indicator for a decrease in trapping efficiency (Heussner et al., 2006). Hence, effects of lateral currents on sampling efficiency of the deeper traps are assumed to be minor. Additionally, tilt meters mounted on the sediment traps did not indicate substantial deviations from vertical, suggesting that hydrodynamic biases on the particle fluxes were minor.

5.1.2. POC and lithogenic content

The export of POC and lithogenic particles is closely associated with total particle fluxes over the complete time series, particularly in the deeper traps (Fig. 2), following observations from other sites in the EMS (Stavrakakis et al., 2013; Pedrosa-Pamies et al., 2021; Van Boxtel et al., 2025). Average POC content of 3.1% in the deepest traps (Table 1) is similar to that at other sites in the EMS (Stavrakakis et al., 2013; Pedrosa-Pamies et al., 2021; Van Boxtel et al., 2025). The sharp decrease in POC between the upper and deeper traps (Table 1) follows the same trends as elsewhere in the EMS (Stavrakakis et al., 2000; Boldrin et al., 2002; Theodosi et al., 2019).

In contrast to POC content, the average lithogenic content of 20.5,

Table 2
Average time-weighted fluxes at the different trap depths of the different deployments.

Measurement	Depth	PS80	BP01	BD03	UN02	NU01	PP01	US02	MP06	CP01
TMF	Upper	10.8	27.8		8.9	29.1			81.5	81.8
	Middle	7.2	10.6	18	3.3	8.3	16.6	23	34.7	16.3
	Lower	3.9	12.9	21.3	13.6	5.4	8.2	10.2	30	22.4
Lithogenic flux	Upper	1.2	5.3		1.4	7.7			24.2	17
	Middle	1	3.5	7.2	0.6	2.5	3.3	4	11.1	3
	Lower	0.4	4.1	3.2	3.5	0.8	2	2.1	12.7	7.1
POC flux	Upper	0.5	1.3			1.3				
	Middle	0.3	0.4			0.5				
	Lower	0.1	0.4			0.2				
PIC flux	Upper	0.4	0.8			0.8				
	Middle	0.3	0.3			0.2				
	Lower	0	0.3			0.2				

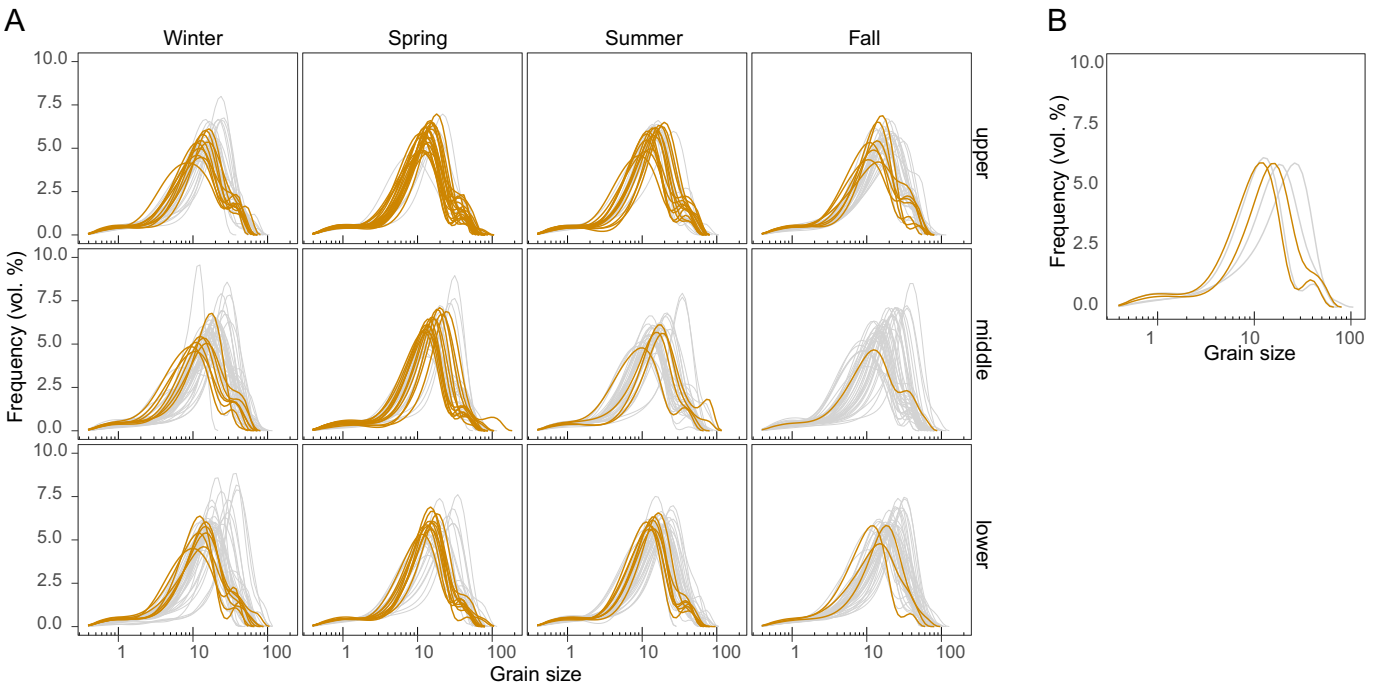


Fig. 3. Grain-size distributions of the sediment trap samples: (A) distributions of all samples in the upper, middle, and lower traps by season; distributions of dust events (>5 mg m^{-2} d^{-1}) are indicated in orange, background dust in grey; and (B) selected distributions typical for dust-event dust (orange) and background dust (grey).

24.9, and 30.7% in the upper, middle, and lower trap, respectively (Table 1) is low compared to other sites in the EMS, where it is generally > 30%, e.g., in the eastern and northern Ionian Sea (Boldrin et al., 2002; Stavrakakis et al., 2013), and can reach up to 86.6% in the deep Ierapetra Basin (Pedrosa-Pamies et al., 2021). Furthermore, it is much lower than ~ 60% reported previously for the same site (Rutten et al., 2000). Differences in lithogenic content are likely due to a difference in the method used for determining the flux of the lithogenic fraction. Lithogenic content in most EMS sediment-trap studies consists of the "residual flux", which is determined by subtracting the biogenic content (organic matter, biogenic silica and biogenic carbonates) from the total particle flux (e.g., Rutten et al., 2000; Boldrin et al., 2002; Stavrakakis et al., 2013; Pedrosa-Pamies et al., 2021). The residual flux likely overestimates the lithogenic content, i.e., quartz, clay minerals and feldspars, as it also contains a non-lithogenic fraction consisting of biogenic phosphates and sulfates, crystal water from the opaline fraction, and OH content of organic matter (Korte et al., 2017; Van der Does et al., 2020). Some other EMS sediment-trap studies (e.g., Rutten et al., 2000; Theodosi et al., 2013) derived the lithogenic fraction from Al, Ti, or Fe content, which relies on assumptions related to the composition and size of lithogenic particles, and might therefore be less accurate than chemically isolated lithogenic fluxes (Van der Does et al., 2020). Indeed, the absolute lithogenic fluxes and lithogenic content in the deepest trap are similar to lithogenic fluxes (0.8–30 mg m^{-2} d^{-1}) and average dust content (27.7%) in the central Ionian Basin (2300 m) obtained with the same chemical isolation method used in this study (Van Boxtel et al., 2025). However, our bulk components, i.e., the lithogenic content, POC content converted to OM, and PIC content converted to $CaCO_3$, only account for ~50% of the TMF. As opal content in sinking particles at the study site is < 1% (Rutten et al., 2000), approximately half of the total flux is unaccounted for. Although the loss of the non-lithogenic fraction of the residual flux might partly explain this difference, it is unlikely that it accounts for approximately half of the total flux. Alternatively, part of the lithogenic fraction might be lost during the procedure used here to chemically isolate the lithogenic fraction, e.g., due to the dissolution of lithogenic carbonates, or the loss of the fine fraction during decanting. However, we deem it unlikely that this can account for such a large loss of lithogenic particles, but it emphasizes the importance of considering the used method when comparing lithogenic content among different sediment-trap datasets. Nevertheless, as all samples have been treated the same, lithogenic fluxes within our records can be compared directly.

5.2. *Relations between atmospheric dust transport and dust export*

5.2.1. *Lithogenic fraction represents Saharan dust*

We here consider the lithogenic fraction to mainly represent Saharan dust, as a major contribution of other sources can be excluded. Fluvial sediment input in the open Ionian Sea is limited in general (Guerzoni et al., 1999), and would only contribute during the wet season from September to May, with peaks in November and December (Poulos and Collins, 2002; Karageorgis et al., 2008; Jilbert et al., 2010). However, maximum lithogenic fluxes in the sediment trap occur during the dry season, when river discharge is low (Fig. 2). Furthermore, Ti/Al ratios of the lithogenic fraction of sinking particles collected at the same site from 1991 to 1994 also indicate that dust is the main source of lithogenic particles, and river input is negligible (Rutten et al., 2000). Additionally, contributions of dust to the EMS from other sources than the Sahara desert are only minor (Guerzoni et al., 1999).

In addition to Saharan dust, atmospheric lithogenic particles can be derived from ashes emitted during volcanic eruptions, particularly from Mount Etna (e.g., Pedrosa-Pamies et al., 2021). However, known eruptions of Mount Etna during the studied interval do not coincide in timing with peaks in lithogenic fluxes in the sediment trap record. Furthermore, the lithogenic fraction of sediment-trap samples collected during volcanic eruptions has a similar orange-brown color and grain-size distribution as other samples, typical for Saharan dust. Hence, although minor contributions of other atmospheric or fluvial sources to the sediment traps cannot be completely excluded, we consider these to be minimal.

5.2.2. *Timing of sediment-trap dust events compared to atmospheric dust transport*

Maximum dust fluxes in spring and summer in the upper trap coincide with atmospheric dust transport indicated by peaks in the monthly

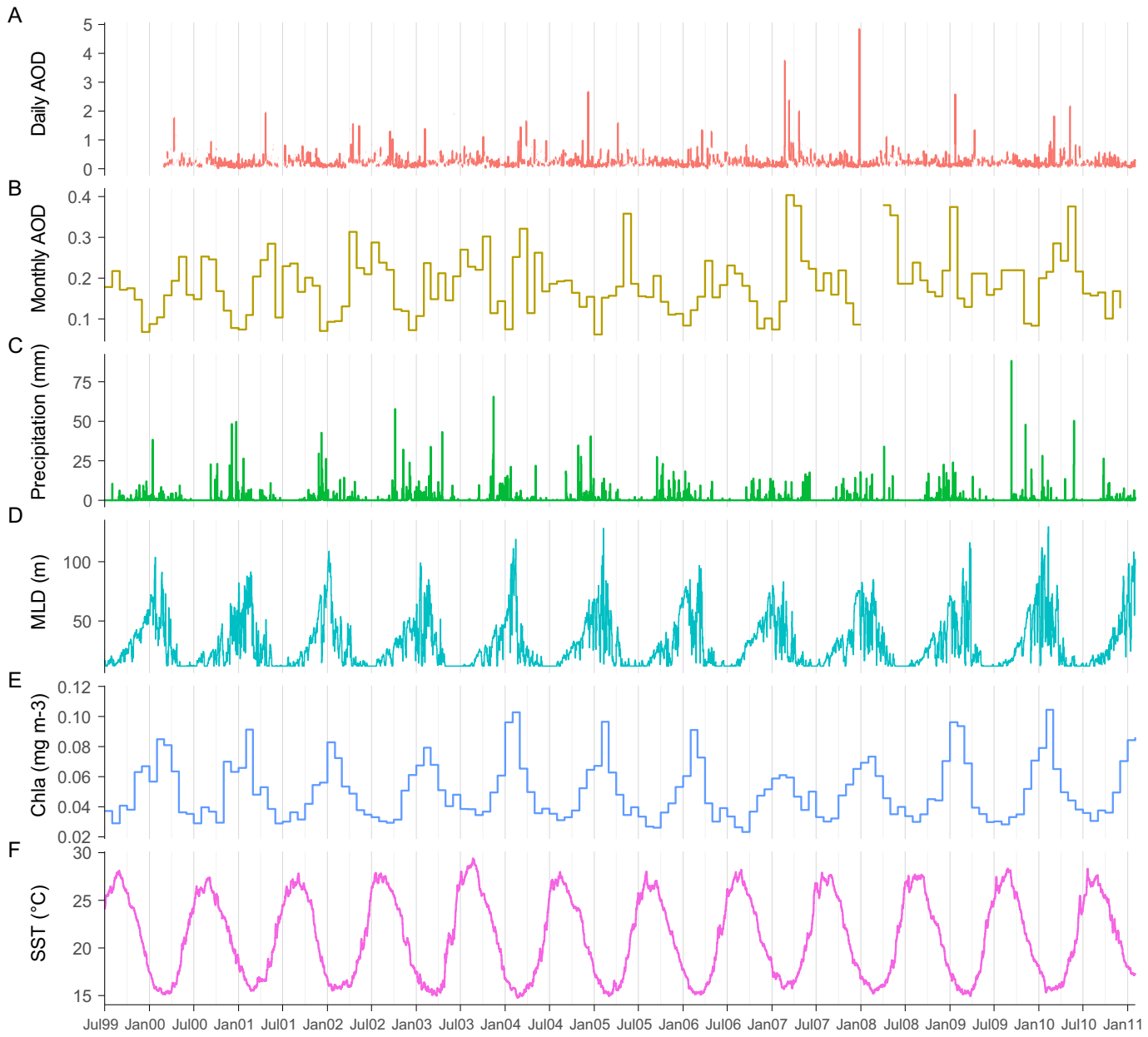


Fig. 4. Time-series of remote-sensing and reanalysis-based oceanographic and atmospheric parameters: (A) daily aerosol optical depth (AOD); (B) monthly AOD; (C) precipitation; (D) mixed layer depth (MLD); (E) chlorophyll *a* concentration in the surface ocean (Chl*a*); (F) sea surface temperature (SST). Line gaps indicate missing values.

AOD record (Fig. 2; Fig. 3) and with the known seasonality of dust transport to the central Mediterranean Sea (Varga et al., 2014). Satellite images further confirm that dust clouds pass the sediment-trap site mainly during spring and summer, supporting the use of AOD to infer atmospheric dust transport, although satellite images may be needed to identify confounding effects of wildfire smoke. Notably, while dust events in the sediment traps can be linked to peaks in AOD, not all peaks in the daily AOD record are also recorded by the sediment traps, particularly in winter, e.g., in January 2003 (Fig. 2, Fig. 4). This either suggests that not all dust transported through the atmosphere over the study site is necessarily deposited, or that dust was deposited on the surface ocean but was not transferred to the sediment traps.

To our knowledge, no direct measurements of surface-ocean dust deposition in proximity to the sediment trap are available for the study period to compare the sediment-trap dust fluxes to. However, high dust and total particle fluxes in spring overlap with maximum dust deposition measured further east on Crete in spring (March – June) from 1988 to 1994 (Mattsson and Nihlén, 1996) and from 1999 to 2005, concomitant with the first part of our sediment record (Theodosi et al., 2019). However, dust deposition on Crete was negligible from June to August (Theodosi et al., 2019), when dust fluxes in the sediment traps at BB are usually high. Nevertheless, seasonal patterns of dust transport vary spatially: where maximum dust transport to the central Mediterranean Sea has a bimodal distribution with peaks from March–May and June–August, dust transport to Crete is at a maximum from March to May and dust clouds usually do not propagate as far eastward as Crete in summer (Israelevich et al., 2002).

5.2.3. *Importance of wet vs dry deposition*

Although there is no data available to differentiate between dust derived from wet or dry deposition, the Bannock Basin sediment-trap record shows that most dust is exported during spring and summer, when precipitation is mostly absent (Fig. 4). Furthermore, most atmospheric dust clouds visible on satellite images are not associated with

major rain clouds. This suggests that dust export peaks in summer are likely mainly associated with dry deposition. Although wet deposition is generally considered the main mode of dust deposited in the Mediterranean Sea, dry deposition accounted for a substantial part of total annual dust deposition measured on land in the western Mediterranean Sea, e.g., on Frioul Island (Laurent et al., 2015), and further east on Lampedusa (Vincent et al., 2016). Alternatively, these summer deposition events could also be associated with small rain events that have the potential to wash out the atmosphere of dust particles but can remain undetected by satellites (Loÿe-Pilot and Martin, 1996).

Notably, the main period of dust export in the sediment-trap record shifts towards winter in 2009 and 2010, concomitant with increased atmospheric dust transport (Fig. 2, Fig. 4). Furthermore, satellite images reveal the occurrence of several large, long-lived atmospheric dust events in December 2008 and January and February 2009 which appear to be substantially longer-lasting and stronger than during the years before the sampling hiatus. These winter dust events coincide with increased precipitation (Fig. 2; Fig. 4). Hence, the winter peaks in TMF and dust-flux events during these later years are most likely the result of wet deposition.

5.3. Vertical transfer of dust particles

Generally, dust flux peaks in the deeper traps occur simultaneously, i.e., in the same bin, or with a difference of one bin. Simultaneous pulses in the middle and lower trap are further confirmed by cross-correlation analysis, which indicates highest correlation at zero time lag for most deployments (Fig. S1). Furthermore, peaks in the deeper traps coincide with peaks in the upper trap for the years when the upper trap was deployed successfully (Fig. 2). This suggests that deposited dust is mainly transferred vertically between the deeper traps. As the depth difference between traps is ~1000 m and sampling resolution ranges from 10 to 23 days, sinking velocities for high-flux events that occur simultaneously at different water depths are at least 40 m d^{-1} for the lowest resolution-, and at least 100 m d^{-1} for the highest-resolution deployments, similar to those obtained from sediment-trap studies in the Ionian Sea (Boldrin et al., 2002; Patara et al., 2009; Stavrakakis et al., 2013; Malinverno et al., 2014). Sinking rates for low-flux intervals are more difficult to constrain as there are no clear peaks that can be linked. However, dust exported during export events (here: >5 mg m^{-2} d^{-1}) comprises >75% of the total dust flux at 1500 and 2500 m. Hence, most of the deposited dust that reaches the deep EMS settles with relatively high sinking velocities.

Dust fluxes are substantially larger in the upper trap than in the deeper traps (Table 1, Fig. 2). This implies that not all dust particles that are deposited at BB are exported vertically. Although dust fluxes also slightly decrease with depth at other sediment-trap sites in the EMS (section 5.1.2) and minor dust events are not always exported to greater depths (e.g., Boldrin et al., 2002; Theodosi et al., 2019), major lithogenic peaks in sediment traps at similar water depth (700 m) are usually transferred to the deeper traps (Theodosi et al., 2019; Tsagkaraki et al., 2020). Given that the largest difference in dust flux occurs between the upper and middle trap, a substantial loss of dust particles occurs after they have left the photic zone. This can possibly be explained by temporary 'storage' of lithogenic particles somewhere in the water column between the upper and middle trap, delaying their export to the sea floor. In the WMS, dust particles without sufficient excess density can be trapped on such a strong density gradient before convective mixing transports them across (Migon et al., 2002; Ternon et al., 2010). In the EMS, strong density gradients exist between the upper and deeper traps, e.g., between the LIW and EMDW (Fig. 1). As large peaks in the deeper traps are always linked to peaks in the upper trap during the same interval, dust events that are 'lost' between the upper and deeper traps are not exported to greater water depths at a later stage but are likely laterally transported away from the trap site.

In addition, some peaks in dust fluxes only occur in the lower trap and are absent in the middle trap, e.g., in spring and summer 2002, and in spring 2009 (Fig. 2). These events might be the result of lateral transport due to resuspension and lateral advection along the slope margins or resuspension of fine material over a deep density gradient, particularly given the small particle sizes that characterizes some of these events, for example in summer 2002 and winter 2010 (Fig. 2). This process was used to explain higher TMFs and coccolith fluxes to deeper traps in the southeast Ionian Sea (Karageorgis et al., 2008; Stavrakakis et al., 2013; Hayat et al., 2022) as well as the occasional occurrence of neritic, benthic and brackish diatom species in deeper sediment traps in the nearby Urania Basin (Malinverno et al., 2014). Alternatively, the occurrence of increased dust fluxes in the lower trap could be a result of 'statistical funneling' combined with heterogeneity in surface ocean conditions due to the complex general and mesoscale circulation (Deuser et al., 1988; Siegel and Deuser, 1997), i.e., the catchment area of the deepest trap is larger and therefore samples are from a larger range of e.g., nutrient concentrations and productivity.

5.4. Characteristics of exported dust

Average flux-weighted modal grain sizes of the dust collected at Bannock Basin (13.4, 15.5 and 14.7 μm, at in the upper, middle, and lower trap, respectively; Table 1) have a similar range as that of Saharan dust particles deposited on Crete (mode of 8–30 μm; Nihlén et al., 1995; Mattsson and Nihlén, 1996) and Corsica (modes ranging from 10 to 30 μm; Guerzoni et al., 1997). However, wind-blown dust is usually well-sorted and has a unimodal distribution (Stuut et al., 2005; Van der Does et al., 2016). The (slight) bimodality in grain-size distributions of most samples could therefore indicate a mixture of different dust events with a distinct grain-size distribution. Alternatively, secondary coarser-grained shoulders in grain-size distributions can be explained by differences in particle shape (Stuut et al., 2005; Friese et al., 2016; Van der Does et al., 2021).

Dust events are typically better sorted than background dust (Fig. 3a; Table 3). This is further supported by end member modeling, which clearly separates high and low dust fluxes based on three end members with modes of 10.3 μm, 19.8 μm, and 34.6 μm, for EM1, EM2, and EM3, respectively, representing 98.5% of the dataset (Fig. S2). Dust events in the deeper traps have a relatively large contribution of EM1 and EM2, while low dust fluxes are associated with a relatively high contribution of EM3. The difference in sorting could be the result of background dust being exported as slowly-settling individual particles in addition to faster-sinking aggregates. For example, individually-settling particles will exhibit different arrival times at the trap depth. In contrast, dust-event dust that is mainly exported in rapidly sinking aggregates would not undergo this sorting by settling speed. Additionally, the dust captured by the sediment traps during low-flux intervals is likely to derive from multiple dust events, with varying particle-size distributions, which could explain the larger standard deviation of the modal grain size of background dust (Table 3).

Other than the differences in grain-size distributions between background dust and dust-event dust, variations in grain size do not show a clear temporal pattern. This deviates from observations from the equatorial North Atlantic, where changes in modal grain size can be linked to seasonal variations in transport routes or altitudes and deposition mechanisms (Friese et al., 2016; Van der Does et al., 2016; Van der Does et al., 2021), and from the nearby Ionian Sea, where interannual variation in modal grain size during spring dust events was linked to different dust transport pathways (Van Boxtel et al., 2025). Notably, the modal grain size of specific dust events is not consistent between the upper, middle and lower trap (Fig. 2). This suggests that the grain-size distribution of deposited dust is altered considerably during transport through the water column at the study site. This would imply that temporal variations in grain-size distributions of dust deposited in the sediment traps do not necessarily reflect changes in e.g., dust sources and transport routes.

Table 3
Descriptive statistics of lithogenic fluxes, modal grain size of the lithogenic fraction, and standard deviation of the grain-size distributions of background dust (lithogenic flux <5 mg m^{-2} d^{-1}) and dust-event dust (lithogenic flux >5 mg m^{-2} d^{-1}) at the different trap depths. Averages correspond to time-weighted averages for fluxes, and flux-weighted averages for the grain-size characteristics. Min: minimum flux; max: maximum flux; sd: standard deviation; n: amount of samples used in the calculations.

Type	Measurement	Depth	Average	min	max	sd	n
Background dust	Lithogenic flux	Upper	1.1	0	4.6	1.2	77
		Middle	1.3	0	4.6	1.1	156
		Lower	1	0	4.5	1.1	145
	Modal grain size	Upper	17.4	7.8	31.5	4.1	75
		Middle	17.8	7.1	38	6	147
		Lower	19	9.4	38	6	142
	SD of grain size distribution	Upper	2.5	2.2	2.7	0.1	75
		Middle	2.5	2.1	2.9	0.1	147
		Lower	2.5	2.1	3	0.1	142
Dust-event dust	Lithogenic flux	Upper	22.1	5	120	22.2	51
		Middle	16.8	5.7	50.3	11.8	32
		Lower	19.1	5.2	59.9	12.3	30
	Modal grain size	Upper	13.5	8.5	19.8	2.4	50
		Middle	14.9	9.4	23.8	3.5	28
		Lower	14.2	10.3	18	2	29
	SD of grain size distribution	Upper	2.5	2.3	2.7	0.1	50
		Middle	2.5	2.3	2.7	0.1	28
		Lower	2.5	2.3	2.7	0.1	29

5.5. Coupled export of dust and POC

For the three years where POC data is available, increased POC fluxes in the two deepest traps coincide with dust events (Fig. 2), supporting the suggestion that dust ballasting of organic aggregates might play an important role in driving POC export in the Mediterranean Sea proposed in earlier work (e.g., Stavrakakis et al., 2013; Tsagaraki et al., 2017; Theodosi et al., 2019). Remarkably, two of the large-flux events in the upper trap that were not transferred to the deeper traps (summer–fall 2000, summer 2005; section 5.3) are associated with largest POC and PIC fluxes (Fig. 2). Furthermore, these events, as well as the spring 2009 and summer 2010 export events (no carbon data available) are associated with highest foraminifer fluxes of the record (Rice, 2025). Hence, increased particle fluxes (POC, PIC, dust and TMF) during these upper-trap events might be associated with ballasting by foraminifer-derived carbonate. The absence of these events in deeper traps could point to a lower efficiency of carbonate ballasting compared to dust ballasting at the study site, for example due to carbonate dissolution, higher organic matter remineralization rates, or a lower excess density of carbonate-ballasted aggregates resulting in lower sinking velocities.

Stokesian settling velocities of ~15 m d^{-1} calculated for the average modal grain size of 14.7 μm for dust in the lower trap are sufficiently high for dust particles to settle individually through the water column. Previous sediment trap studies in the Mediterranean Sea that observed a link between POC and dust export have argued that dust particles are too small to settle individually, such as in the WMS, where dust export seems to be ultimately driven by hydrological processes (Migon et al., 2002; Heimbürger et al., 2013) and the EMS, where the availability of POC was proposed to ultimately drive dust export (Tsagkaraki et al., 2020). However, these studies did not directly measure the grain-size distribution of the collected dust fraction, but instead were either based on settling velocities of the size distribution of PM_{10} atmospheric dust measured over the EMS (Gerasopoulos et al., 2007), or based on the assumption that settling dust particles had grain sizes <3.9 μm (Deuser et al., 1983) or < 5 μm (Buat-Ménard et al., 1989) that have negligible Stokesian settling velocities and are too small to sink individually. Nevertheless, while the average modal grain sizes of settling dust particles collected at Bannock Basin and the settling velocities based on Stokes' Law are sufficiently large for individual lithogenic particles to be transferred to the deep EMS on reasonable timescales, they are too low to explain settling velocities of at least 40 m d^{-1} during high flux events (section 5.3). Instead, the co-occurrence of peaks in dust and POC fluxes in the deeper sediment traps (Fig. 2) suggests that dust and POC are exported together in larger and heavier dust-ballasted organic aggregates, facilitated by the combination of dust deposition and the simultaneous presence of organic aggregates in the surface ocean.

5.6. Seasonality of coupled dust-POC export

Considering the seasonality in particle fluxes and the close association between POC, dust, and TMF at our study site, combined with seasonal oceanographic changes and associated dynamics of primary productivity (Fig. 4), we hypothesize that the timing of dust deposition in relation to primary production is important for the simultaneous export of both. The regular export maxima to the deeper traps that occur every year during spring and early summer for the first part of the record, i.e., from 2000 to 2004 (Fig. 2), are consistent with the timing of maximum TMFs and/or dust fluxes in other sediment traps in the Ionian Sea (Rutten et al., 2000; Van Boxtel et al., 2025) and the wider oligotrophic EMS (Boldrin et al., 2002; Stavrakakis et al., 2013; Theodosi et al., 2019; Pedrosa-Pamies et al., 2021). Consistent export pulses of POC and dust in spring and early summer might be associated with the concurrent increase of atmospheric dust transport (Fig. 4), and the formation of organic aggregates in the surface ocean at the end of the increase in surface ocean productivity from January–April that characterizes large parts of the EMS including the southern Ionian Sea (D'Ortenzio and Ribera D'Alcalà, 2009). However, although small increases in dust flux and TMF are visible in spring every year, the magnitude, duration, and exact timing of these annual spring peaks vary substantially between years (Fig. 2). Differences in the exact timing and amplitude of the seasonal dust export peaks might be associated with differences in dust deposition between years. Nevertheless, the timing of dust transport over the trap site was similar between years with low and high dust fluxes according to AOD (Fig. 4), although differences in actual deposition or deposition mode (wet vs dry) cannot be excluded. Alternatively, interannual differences in the timing and magnitude of dust, TMF, and POC export could also be due to the large spatial heterogeneity in the hydrological and biological conditions in the surface EMS, which result in large spatial differences in productivity and circulation patterns.

While the occurrence of the spring export pulses might be associated with increased OM availability in the surface ocean, export pulses can continue well into summer (e.g., in 2000–2002 and 2004; Fig. 2), indicating that substantial dust and POC export can also occur under stratified conditions. Although not detected by satellites, primary production still occurs deeper in the photic zone, below the first optical

depth, corresponding to ~15–35 m water depth in the Mediterranean Sea (D'Ortenzio and Ribera D'Alcalà, 2009). Hence, dust-ballasted aggregates in summer could also be formed with POC produced deeper in the photic zone. Finally, primary productivity during summer could have been enhanced as a result of dust fertilization.

Low dust fluxes in the sediment traps during fall and winter coincide with minimum atmospheric dust transport. However, episodic dust deposition still occurs, e.g., in winter 2003 (section 5.2.2; Fig. 4). Limited aggregate formation in winter might explain why during most years, dust deposited during winter is not (directly) transferred to the sediment trap. Additionally, summer surface circulation patterns (anticyclonic eddies and associated downwelling) are more favorable for export than winter circulation patterns (jet-stream) (Estournel et al., 2021). Notably, in 2009 and 2010, highest dust fluxes of the year occur during winter, and also average dust fluxes for these years are much larger compared to the earlier sampling interval (Fig. 2; Table 2). Although the upper traps are placed within a narrow same depth range during all deployments, the upper traps were located ~200 m higher in the water column from 2008 to 2011 than during the earlier deployments (Table S1). Hence, the year-round high dust fluxes in the upper trap during the later deployments could be due to a change in water masses surrounding the sediment traps (LIW instead of TMF or EMDW; Poulos, 2023). Nonetheless, the shift in timing of the main export peak in the deeper traps cannot be explained by a change in the deployment depth of the upper trap, and must be due to interannual variations in the driver of dust export.

The change in timing of dust export observed in 2009 and 2010 could be a result of the switch in BiOS regime from cyclonic to an anticyclonic circulation of the NIG that occurred between 2006 and 2010. This switch resulted in changes in upwelling and downwelling patterns in the basin (Gačić et al., 2010; Civitarese et al., 2023) which affected primary production and its timing in other sites in the Ionian Sea (Civitarese et al., 2010; Lavigne et al., 2018). Although the BiOS transitional years are missing in our record, a progressive increase in TMF, dust, and POC fluxes in sediment traps at the NESTOR site (eastern Ionian Sea) from 2006 to 2010 has also been attributed to this change in BiOS regime (Stavrakakis et al., 2013). Furthermore, dust fluxes at this site in 2010 also peak in winter instead of spring. However, sediment-trap records from the Bannock Basin covering 1991–1994, during a similar BiOS regime with general anticyclonic circulation in the Ionian Sea, do not show increased export during winter. Hence, the large export events at Bennock Basin in winter 2009 and 2010 could also be a result of the exceptionally strong and long-lived dust events that occurred in fall and winter 2009 and winter 2010 (section 5.2.2). Possibly, the long duration and high intensity of the dust events from November 2008–2009 (section 5.2.3) could have had fertilizing effects resulting in POC availability, and/or provided sufficient ballast to export POC present in the surface ocean.

6. Conclusions

Increased lithogenic fluxes in the upper trap from early spring to early fall coincide with the seasons of atmospheric dust transport, indicating that dust particles that are transferred to the deep EMS are exported relatively rapidly upon deposition. Furthermore, the simultaneous occurrence of peak lithogenic fluxes at the different trap depths during spring and early summer indicates rapid sinking velocities. However, not all dust is transferred to the deep EMS: some large dust pulses occur in the upper trap but not in the deeper traps; average modal grain size increases with trap depth; and some large atmospheric dust events are absent in the sediment traps. The close association between lithogenic flux, TMF, and POC flux indicates simultaneous export and hence a coupled export mechanism. Although grain sizes of the dust collected by the sediment traps are sufficiently large to allow for export of individual dust particles with reasonable sinking velocities, calculated settling rates during peak dust fluxes are faster than Stokesian settling rates of the individual dust particles. This, combined with the coincidence of dust export pulses with increased POC fluxes, suggests that dust particles are mainly exported as dust-ballasted organic aggregates, which implies that dust can act as ballast for POC export. However, sufficient POC in the surface ocean is required for large amounts of dust export to take place in the EMS. Ultimately, the timing of dust deposition in relation to primary production seems to determine whether the deposited dust is transferred to the deep ocean. This implies that dust deposition in spring and summer might contribute to vertical carbon export during these seasons, but dust deposited during other seasons is usually not exported and thus does not affect vertical POC export. Nevertheless, a shift to maximum dust fluxes in winter 2009 and 2010 shows that export of dust is not always restricted to spring and early summer, and suggests that very large dust events might still trigger carbon export by fertilization in other seasons.

CRediT authorship contribution statement

Anouk P.E. van Boxtel: Writing – original draft, Visualization, Validation, Project administration, Methodology, Investigation, Formal analysis, Data curation, Conceptualization. **Addison Rice:** Writing – review & editing, Validation, Methodology, Investigation, Data curation. **Constantijn Kurpershoek:** Writing – review & editing, Investigation, Data curation. **Tijno de Nooij:** Writing – review & editing, Investigation, Data curation. **Gert J. de Lange:** Writing – review & editing, Resources, Funding acquisition, Data curation. **Francien Peterse:** Writing – review & editing, Supervision, Resources, Methodology, Funding acquisition, Conceptualization. **Jan-Berend W. Stuut:** Writing – review & editing, Supervision, Resources, Methodology, Funding acquisition, Conceptualization.

Declaration of competing interest

The authors declare the following financial interests/personal relationships which may be considered as potential competing interests: Given their role as editor-in-chief of Aeolian Research, Jan-Berend W. Stuut had no involvement in the peer-review of this article and has no access to information regarding its peer-review. Full responsibility for the editorial process for this article was delegated to another journal editor. If there are other authors, they declare that they have no known competing financial interests or personal relationships that could have appeared to influence the work reported in this paper.

Acknowledgements

The authors thank NIOZ crew and technicians for mooring and recovery of the Bannock Basin sediment traps; P. van Santvoort and this team for on-board sample splitting; and D. Eefting, A. van Dijk, P. van Gaever and J. Kooijman for their assistance in the lab. The authors also thank F. Mienis for insightful discussions regarding the data. This study has been conducted using E.U. Copernicus Marine Service Information. AOD and precipitation analyses used in this paper were produced with the Giovanni online data system, developed and maintained by the NASA GES DISC. We further acknowledge the use of imagery from the Worldview Snapshots application (https://wvs.earthdata.nasa.gov), part of the Earth Observing System Data and Information System (EOSDIS), and the MODIS mission scientists and associated NASA personnel for the data used in this research effort. This project was funded by the UU-NIOZ project NZ4543.28, funded by Utrecht University. This manuscript has benefitted from feedback by two anonymous reviewers and the editor.

Appendix A. Supplementary data

Supplementary data to this article can be found online at https://doi.org/10.1016/j.aeolia.2026.101070.

Data availability

The data have been stored in ZENODO: https://doi.org/10.5281/zenodo.20049533.

Sediment-trap bulk fluxes, dust properties, and grain-size distributions at Bannock Basin, Ionian Sea (Original data) (ZENODO)

References

Armstrong, R.A., Lee, C., Hedges, J.I., Honjo, S., Wakeham, S.G., 2002. A new, mechanistic model for organic carbon fluxes in the ocean based on the quantitative association of POC with ballast minerals. Deep-Sea Res. II Top. Stud. Oceanogr. 49 (1–3), 219–236. https://doi.org/10.1016/S0967-0645(01)00101-1.

Berline, L., Doglioli, A.M., Petrenko, A., Barrillon, S., Espinasse, B., Le Moigne, F.A.C., Simon-Bot, F., Thyssen, M., Carlotti, F., 2021. Long-distance particle transport to the central Ionian Sea. Biogeosciences 18 (24), 6377–6392. https://doi.org/10.5194/bg-18-6377-2021.

Boldrin, A., Miserocchi, S., Rabitti, S., Turchetto, M., Balboni, V., Socal, G., 2002. Particulate matter in the southern Adriatic and Ionian Sea: characterisation and downward fluxes. J. Mar. Syst. 33, 389–410. https://doi.org/10.1016/S0924-7963(02)00068-4.

Buat-Ménard, P., Davies, J., Remoudaki, E., Miquel, J.C., Bergametti, G., Lambert, C.E., Ezat, U., Quetel, C., La Rosa, J., Fowler, S.W., 1989. Non-steady-state biological removal of atmospheric particles from Mediterranean surface waters. Nature 340 (6229), 131–134. https://doi.org/10.1038/340131a0.

Buesseler, K.O., Antia, A.N., Chen, M., Fowler, S.W., Gardner, W.D., Gustafsson, O., Harada, K., Michaels, A.F., Rutgers van der Loeff, M., Sarin, M., 2007. An assessment of the use of sediment traps for estimating upper ocean particle fluxes. J. Mar. Res. 65 (3), 345–416.

Casotti, R., Landolfi, A., Brunet, C., D'Ortenzio, F., Mangoni, O., Ribera D'Alcalà, M., Denis, M., 2003. Composition and dynamics of the phytoplankton of the Ionian Sea (eastern Mediterranean). J. Geophys. Res. Oceans 108 (C9). https://doi.org/10.1029/2002jc001541.

Civitarese, G., Gačić, M., Lipizer, M., Eusebi Borzelli, G.L., 2010. On the impact of the bimodal oscillating system (BiOS) on the biogeochemistry and biology of the Adriatic and Ionian seas (eastern Mediterranean). Biogeosciences 7 (12), 3987–3997. https://doi.org/10.5194/bg-7-3987-2010.

Civitarese, G., Gačić, M., Batistić, M., Bensi, M., Cardin, V., Dulčić, J., Garić, R., Menna, M., 2023. The BiOS mechanism: history, theory, implications. Prog. Oceanogr. 216. https://doi.org/10.1016/j.pocean.2023.103056.

Crouvi, O., Schepanski, K., Amit, R., Gillespie, A.R., Enzel, Y., 2012. Multiple dust sources in the Sahara Desert: the importance of sand dunes. Geophys. Res. Lett. 39 (13). https://doi.org/10.1029/2012gl052145.

De La Rocha, C.L., Passow, U., 2007. Factors influencing the sinking of POC and the efficiency of the biological carbon pump. Deep-Sea Res. II Top. Stud. Oceanogr. 54 (5–7), 639–658. https://doi.org/10.1016/j.dsr2.2007.01.004.

Deuser, W.G., Brewer, P.G., Jickells, T.D., Commeau, R.F., 1983. Biological control of the removal of abiogenic particles from the Surface Ocean. Science 219 (4583), 388–391. https://doi.org/10.1126/science.219.4583.388.

Deuser, W.G., Muller-Karger, F.E., Hemleben, C., 1988. Temporal variations of particle fluxes in the deep subtropical and tropical North Atlantic: Eulerian versus Lagrangian effects. J. Geophys. Res. Oceans 93 (C6), 6857–6862. https://doi.org/10.1029/jc093ic06p06857.

D'Ortenzio, F., Ribera D'Alcalà, M., 2009. On the trophic regimes of the Mediterranean Sea: a satellite analysis. Biogeosciences 6 (2), 139–148. https://doi.org/10.5194/bg-6-139-2009.

D'Ortenzio, F., Iudicone, D., De Boyer Montegut, C., Testor, P., Antoine, D., Marullo, S., Santoleri, R., Madec, G., 2005. Seasonal variability of the mixed layer depth in the Mediterranean Sea as derived from in situ profiles. Geophys. Res. Lett. 32 (12). https://doi.org/10.1029/2005gl022463.

Estournel, C., Marsaleix, P., Ulses, C., 2021. A new assessment of the circulation of Atlantic and intermediate waters in the eastern Mediterranean. Prog. Oceanogr. 198. https://doi.org/10.1016/j.pocean.2021.102673.

Francois, R., Honjo, S., Krishfield, R., Manganini, S., 2002. Factors controlling the flux of organic carbon to the bathypelagic zone of the ocean. Glob. Biogeochem. Cycles 16 (4). https://doi.org/10.1029/2001gb001722.

Friese, C.A., Van der Does, M., Merkel, U., Iversen, M.H., Fischer, G., Stuut, J.-B.W., 2016. Environmental factors controlling the seasonal variability in particle size distribution of modern Saharan dust deposited off cape blanc. Aeolian Res. 22, 165–179. https://doi.org/10.1016/j.aeolia.2016.04.005.

Gačić, M., Borzelli, G.L.E., Civitarese, G., Cardin, V., Yari, S., 2010. Can internal processes sustain reversals of the ocean upper circulation? The Ionian Sea example. Geophys. Res. Lett. 37 (9). https://doi.org/10.1029/2010gl043216.

Gačić, M., Civitarese, G., Eusebi Borzelli, G.L., Kovačević, V., Poulain, P.M., Theocharis, A., Menna, M., Catucci, A., Zarokanellos, N., 2011. On the relationship between the decadal oscillations of the northern Ionian Sea and the salinity distributions in the eastern Mediterranean. J. Geophys. Res. 116 (C12). https://doi.org/10.1029/2011jc007280.

Gerasopoulos, E., Koulouri, E., Kalivitis, N., Kouvarakis, G., Saarikoski, S., Mäkelä, T., Hillamo, R., Mihalopoulos, N., 2007. Size-segregated mass distributions of aerosols over eastern Mediterranean: seasonal variability and comparison with AERONET columnar size-distributions. Atmos. Chem. Phys. 7 (10), 2551–2561. https://doi.org/10.5194/acp-7-2551-2007.

Guerreiro, C.V., Baumann, K.H., Brummer, G.J.A., Valente, A., Fischer, G., Ziveri, P., Brotas, V., Stuut, J.B.W., 2021. Carbonate fluxes by coccolithophore species between NW Africa and the Caribbean: implications for the biological carbon pump. Limnol. Oceanogr. 66 (8), 3190–3208. https://doi.org/10.1002/lno.11872.

Guerzoni, S., Molinaroli, E., Chester, R., 1997. Saharan dust inputs to the western Mediterranean Sea: depositional patterns, geochemistry and sedimentological implications. Deep-Sea Res. II Top. Stud. Oceanogr. 44 (3–4), 631–654. https://doi.org/10.1016/s0967-0645(96)00096-3.

Guerzoni, S., Chester, R., Dulac, F., Herut, B., Loye-Pilot, M.-D., Measures, C., Migon, C., Molinaroli, E., Moulin, C., Rossini, P., Saydam, C., Soudine, A., Ziveri, P., 1999. The role of atmospheric deposition in the biogeochemistry of the Mediterranean Sea. Prog. Oceanogr. 44 (1–3), 147–190. https://doi.org/10.1016/S0079-6611(99)00024-5.

Guieu, C., Aumont, O., Paytan, A., Bopp, L., Law, C.S., Mahowald, N., Achterberg, E.P., Marañón, E., Salihoglu, B., Crise, A., Wagener, T., Herut, B., Desboeufs, K., Kanakidou, M., Olgun, N., Peters, F., Pulido-Villena, E., Tovar-Sanchez, A., Völker, C., 2014. The significance of the episodic nature of atmospheric deposition to low nutrient low chlorophyll regions. Glob. Biogeochem. Cycles 28 (11), 1179–1198. https://doi.org/10.1002/2014gb004852.

Hayat, S., Skampa, E., Gogou, A., Stavrakakis, S., Parinos, C., Triantaphyllou, M., 2022. Seasonal variability in present-day coccolithophore fluxes in deep eastern Mediterranean Sea: a multi-year study (2015–2017) of coccolithophore export in SE Ionian Sea at 4300 m depth. J. Mar. Sci. Eng. 10 (1761). https://doi.org/10.3390/jmse10111761.

Heimbürger, L.-E., Lavigne, H., Migon, C., D'Ortenzio, F., Estournel, C., Coppola, L., Miquel, J.-C., 2013. Temporal variability of vertical export flux at the DYFAMED time-series station (northwestern Mediterranean Sea). Prog. Oceanogr. 119, 59–67. https://doi.org/10.1016/j.pocean.2013.08.005.

Heussner, S., Durrieu de Madron, X., Calafat, A., Canals, M., Carbonne, J., Delsaut, N., Saragoni, G., 2006. Spatial and temporal variability of downward particle fluxes on a continental slope: lessons from an 8-yr experiment in the Gulf of Lions (NW Mediterranean). Mar. Geol. 234 (1), 63–92. https://doi.org/10.1016/j.margeo.2006.09.003.

Israelevich, P.L., Levin, Z., Joseph, J.H., Ganor, E., 2002. Desert aerosol transport in the Mediterranean region as inferred from the TOMS aerosol index. J. Geophys. Res. Atmos. 107 (D21). https://doi.org/10.1029/2001jd002011.

Israelevich, P., Ganor, E., Alpert, P., Kishcha, P., Stupp, A., 2012. Predominant transport paths of Saharan dust over the Mediterranean Sea to Europe. J. Geophys. Res. Atmos. 117 (D2). https://doi.org/10.1029/2011JD016482.

Iversen, M.H., 2023. Carbon export in the ocean: a biologist's perspective. Annu. Rev. Mar. Sci. 15 (1), 357–381. https://doi.org/10.1146/annurev-marine-032122-035153.

Iversen, M.H., Robert, M.L., 2015. Ballasting effects of smectite on aggregate formation and export from a natural plankton community. Mar. Chem. 175, 18–27. https://doi.org/10.1016/j.marchem.2015.04.009.

Jilbert, T., Reichart, G.-J., Aeschlimann, B., Günther, D., Boer, W., De Lange, G., 2010. Climate-controlled multidecadal variability in north African dust transport to the Mediterranean. Geology 38 (1), 19–22. https://doi.org/10.1130/g25287.1.

Karageorgis, A.P., Gardner, W.D., Georgopoulos, D., Mishonov, A.V., Krasakopoulou, E., Anagnostou, C., 2008. Particle dynamics in the eastern Mediterranean Sea: a synthesis based on light transmission, PMC, and POC archives (1991–2001). Deep-Sea Res. I Oceanogr. Res. Pap. 55 (2), 177–202. https://doi.org/10.1016/j.dsr.2007.11.002.

Klaas, C., Archer, D.E., 2002. Association of sinking organic matter with various types of mineral ballast in the deep sea: implications for the rain ratio. Glob. Biogeochem. Cycles 16 (4). https://doi.org/10.1029/2001gb001765.

Komada, T., Anderson, M.R., Dorfmeier, C.L., 2008. Carbonate removal from coastal sediments for the determination of organic carbon and its isotopic signatures, $\delta^{13}C$ and $\Delta^{14}C$: comparison of fumigation and direct acidification by hydrochloric acid. Limnol. Oceanogr. Methods 6 (6), 254–262. https://doi.org/10.4319/lom.2008.6.254.

Korte, L.F., Brummer, G.-J.A., Van der Does, M., Guerreiro, C.V., Hennekam, R., Van Hateren, J.A., Jong, D., Munday, C.I., Schouten, S., Stuut, J.-B.W., 2017. Downward particle fluxes of biogenic matter and Saharan dust across the equatorial North Atlantic. Atmos. Chem. Phys. 17 (9), 6023–6040. https://doi.org/10.5194/acp-17-6023-2017.

Krom, M.D., Groom, S., Zohary, T., 2003. The eastern Mediterranean. In: Black, K.D., Shimmield, G.B. (Eds.), Biogeochemistry of Marine Systems. Blackwell, pp. 91–122. https://doi.org/10.1201/9780367812423-4.

Krom, M.D., Herut, B., Mantoura, R.F.C., 2004. Nutrient budget for the eastern Mediterranean: implications for phosphorus limitation. Limnol. Oceanogr. 49 (5), 1582–1592. https://doi.org/10.4319/lo.2004.49.5.1582.

Laurent, B., Losno, R., Chevaillier, S., Vincent, J., Roullet, P., Bon Nguyen, E., Ouboulmane, N., Triquet, S., Fornier, M., Raimbault, P., Bergametti, G., 2015. An automatic collector to monitor insoluble atmospheric deposition: application for mineral dust deposition. Atmos. Meas. Tech. 8 (7), 2801–2811. https://doi.org/10.5194/amt-8-2801-2015.

Lavigne, H., Civitarese, G., Gačić, M., D'Ortenzio, F., 2018. Impact of decadal reversals of the north Ionian circulation on phytoplankton phenology. Biogeosciences 15 (14), 4431–4445. https://doi.org/10.5194/bg-15-4431-2018.

Lee, C., Peterson, M.L., Wakeham, S.G., Armstrong, R.A., Cochran, J.K., Miquel, J.C., Fowler, S.W., Hirschberg, D., Beck, A., Xue, J., 2009. Particulate organic matter and ballast fluxes measured using time-series and settling velocity sediment traps in the

northwestern Mediterranean Sea. Deep-Sea Res. II Top. Stud. Oceanogr. 56 (18), 1420–1436. https://doi.org/10.1016/j.dsr2.2008.11.029.
Louis, J., Pedrotti, M.L., Gazeau, F., Guieu, C., 2017. Experimental evidence of formation of transparent exopolymer particles (TEP) and POC export provoked by dust addition under current and high pCO2 conditions. PLoS One 12 (2). https://doi.org/10.1371/journal.pone.0171980.
Loÿe-Pilot, M.D., Martin, J.M., 1996. Saharan dust input to the Western Mediterranean: An eleven years record in Corsica. In: Guerzoni, S., Chester, R. (Eds.), The Impact of Desert Dust across the Mediterranean. Springer Netherlands, pp. 191–199. https://doi.org/10.1007/978-94-017-3354-0_18.
Malinverno, E., Maffioli, P., Corselli, C., De Lange, G.J., 2014. Present-day fluxes of coccolithophores and diatoms in the pelagic Ionian Sea. J. Mar. Syst. 132, 13–27. https://doi.org/10.1016/j.jmarsys.2013.12.009.
Marañón, E., Van Wambeke, F., Uitz, J., Boss, E.S., Dimier, C., Dinasquet, J., Engel, A., Haëntjens, N., Pérez-Lorenzo, M., Taillandier, V., Zäncker, B., 2021. Deep maxima of phytoplankton biomass, primary production and bacterial production in the Mediterranean Sea. Biogeosciences 18 (5), 1749–1767. https://doi.org/10.5194/bg-18-1749-2021.
Mattsson, J.O., Nihlén, T., 1996. The transport of Saharan dust to southern Europe: a scenario. J. Arid Environ. 32 (2), 111–119. https://doi.org/10.1006/jare.1996.0011.
McGregor, H.V., Dupont, L., Stuut, J.-B.W., Kuhlmann, H., 2009. Vegetation change, goats, and religion: a 2000-year history of land use in southern Morocco. Quat. Sci. Rev. 28 (15–16), 1434–1448. https://doi.org/10.1016/j.quascirev.2009.02.012.
Migon, C., Sandroni, V., Marty, J.-C., Gasser, B., Miquel, J.-C., 2002. Transfer of atmospheric matter through the euphotic layer in the northwestern Mediterranean: seasonal pattern and driving forces. Deep-Sea Res. II Top. Stud. Oceanogr. 49 (11), 2125–2141. https://doi.org/10.1016/S0967-0645(02)00031-0.
Moulin, C., Lambert, C.E., Dayan, U., Masson, V., Ramonet, M., Bousquet, P., Legrand, M., Balkanski, Y.J., Guelle, W., Marticorena, B., Bergametti, G., Dulac, F., 1998. Satellite climatology of African dust transport in the Mediterranean atmosphere. J. Geophys. Res. Atmos. 103 (D11). https://doi.org/10.1029/98jd00171.
Nihlén, T., Mattsson, J.O., Rapp, A., Gagaoudaki, C., Kornaros, G., Papageorgiou, J., 1995. Monitoring of Saharan dust fallout on Crete and its contribution to soil formation. Tellus Ser. B Chem. Phys. Meteorol. 47 (3), 365. https://doi.org/10.3402/tellusb.v47i3.16055.
Pabortsava, K., Lampitt, R.S., Benson, J., Crowe, C., McLachlan, R., Le Moigne, F.A.C., Mark Moore, C., Pebody, C., Provost, P., Rees, A.P., Tilstone, G.H., Woodward, E.M. S., 2017. Carbon sequestration in the deep Atlantic enhanced by Saharan dust. Nat. Geosci. 10 (3), 189–194. https://doi.org/10.1038/ngeo2899.
Passow, U., De La Rocha, C.L., Fairfield, C., Schmidt, K., 2014. Aggregation as a function of PCO2 and mineral particles. Limnol. Oceanogr. 59 (2), 532–547. https://doi.org/10.4319/lo.2014.59.2.0532.
Patara, L., Pinardi, N., Corselli, C., Malinverno, E., Tonani, M., Santoleri, R., Masina, S., 2009. Particle fluxes in the deep eastern Mediterranean basins: the role of ocean vertical velocities. Biogeosciences 6 (3), 333–348. https://doi.org/10.5194/bg-6-333-2009.
Paterson, G.A., Heslop, D., 2015. New methods for unmixing sediment grain size data. Geochem. Geophys. Geosyst. 16 (12), 4494–4506. https://doi.org/10.1002/2015gc006070.
Pedrosa-Pamies, R., Parinos, C., Sanchez-Vidal, A., Calafat, A., Canals, M., Velaoras, D., Mihalopoulos, N., Kanakidou, M., Lampadariou, N., Gogou, A., 2021. Atmospheric and oceanographic forcing impact particle flux composition and carbon sequestration in the eastern Mediterranean Sea: a three-year time-series study in the deep Ierapetra Basin. Front. Earth Sci. 9. https://doi.org/10.3389/feart.2021.591948.
Pinardi, N., Zavatarelli, M., Adani, M., Coppini, G., Fratianni, C., Oddo, P., Simoncelli, S., Tonani, M., Lyubartsev, V., Dobricic, S., Bonaduce, A., 2015. Mediterranean Sea large-scale low-frequency ocean variability and water mass formation rates from 1987 to 2007: a retrospective analysis. Prog. Oceanogr. 132, 318–332. https://doi.org/10.1016/j.pocean.2013.11.003.
Ploug, H., Iversen, M.H., Fischer, G., 2008a. Ballast, sinking velocity, and apparent diffusivity within marine snow and zooplankton fecal pellets: implications for substrate turnover by attached bacteria. Limnol. Oceanogr. 53 (5), 1878–1886. https://doi.org/10.4319/lo.2008.53.5.1878.
Ploug, H., Iversen, M.H., Koski, M., Buitenhuis, E.T., 2008b. Production, oxygen respiration rates, and sinking velocity of copepod fecal pellets: direct measurements of ballasting by opal and calcite. Limnol. Oceanogr. 53 (2), 469–476. https://doi.org/10.4319/lo.2008.53.2.0469.
Poulos, S.E., 2023. Water masses of the Mediterranean Sea and Black Sea: an overview. Water 15 (18), 3194. https://doi.org/10.3390/w15183194.
Poulos, S.E., Collins, M.B., 2002. Fluviatile sediment fluxes to the Mediterranean Sea: a quantitative approach and the influence of dams. Geol. Soc. Lond. Spec. Publ. 191 (1), 227–245. https://doi.org/10.1144/gsl.sp.2002.191.01.16.
Prospero, J.M., Ginoux, P., Torres, O., Nicholson, S.E., Gill, T.E., 2002. Environmental characterization of global sources of atmospheric soil dust identified with the nimbus 7 total ozone mapping spectrometer (TOMS) absorbing aerosol product. Rev. Geophys. 40 (1), 2-1-2-31. https://doi.org/10.1029/2000rg000095.
Rice, A., 2025. *Probing Paleoceanographic Proxies* [PhD Thesis, Utrecht University]. Utrecht.
Rutten, A., De Lange, G., Ziveri, P., Thomson, J., Van Santvoort, P., Colley, S., Corselli, C., 2000. Recent terrestrial and carbonate fluxes in the pelagic eastern Mediterranean; a comparison between sediment trap and surface sediment. Palaeogeogr. Palaeoclimatol. Palaeoecol. 158 (3–4), 197–213. https://doi.org/10.1016/S0031-0182(00)00050-X.
Schroeder, K., Ben Ismail, S., Bensi, M., Bosse, A., Chiggiato, J., Civitarese, G., Falcieri, M.F., Fusco, G., Gačić, M., Gertman, I., Kubin, E., Malanotte-Rizzoli, P., Martellucci, R., Menna, M., Ozer, T., Taupier-Letage, I., Vargas-Yáñez, M., Velaoras, D., Vilibić, I., 2024. A consensus-based, revised and comprehensive catalogue for Mediterranean water masses acronyms. Mediterr. Mar. Sci. 25 (3), 783–791. https://doi.org/10.12681/mms.38736.
Siegel, D.A., Deuser, W.G., 1997. Trajectories of sinking particles in the Sargasso Sea: modeling of statistical funnels above deep-ocean sediment traps. Deep-Sea Res. I Oceanogr. Res. Pap. 44 (9), 1519–1541. https://doi.org/10.1016/S0967-0637(97)00028-9.
Siokou-Frangou, I., Christaki, U., Mazzocchi, M.G., Montresor, M., Ribera D'Alcalá, M., Vaqué, D., Zingone, A., 2010. Plankton in the open Mediterranean Sea: a review. Biogeosciences 7 (5), 1543–1586. https://doi.org/10.5194/bg-7-1543-2010.
Skliris, N., 2014. Past, present and future patterns of the thermohaline circulation and characteristic water masses of the Mediterranean Sea. In: Dubinsky, S.G.Z. (Ed.), The Mediterranean Sea its History and Present Challenges. Springer, pp. 29–48. https://doi.org/10.1007/978-94-007-6704-1_3.
Stavrakakis, S., Chronis, G., Tselepides, A., Heussner, S., Monaco, A., Abassi, A., 2000. Downward fluxes of settling particles in the deep Cretan Sea (NE Mediterranean). Prog. Oceanogr. 46 (2–4), 217–240. https://doi.org/10.1016/s0079-6611(00)00020-3.
Stavrakakis, S., Gogou, A., Krasakopoulou, E., Karageorgis, A.P., Kontoyiannis, H., Rousakis, G., Velaoras, D., Perivoliotis, L., Kambouri, G., Stavrakaki, I., Lykousis, V., 2013. Downward fluxes of sinking particulate matter in the deep Ionian Sea (NESTOR site), eastern Mediterranean: seasonal and interannual variability. Biogeosciences 10 (11), 7235–7254. https://doi.org/10.5194/bg-10-7235-2013.
Stuut, J.-B.W., Zabel, M., Ratmeyer, V., Helmke, P., Schefuß, E., Lavik, G., Schneider, R. R., 2005. Provenance of present-day eolian dust collected off NW Africa. J. Geophys. Res. 110, D04202. https://doi.org/10.1029/2004JD005161.
Stuut, J.-B., Smalley, I., O'Hara-Dhand, K., 2009. Aeolian dust in Europe: African sources and European deposits. Quat. Int. 198 (1–2), 234–245. https://doi.org/10.1016/j.quaint.2008.10.007.
Tegen, I., Harrison, S.P., Kohfeld, K., Prentice, I.C., Coe, M., Heimann, M., 2002. Impact of vegetation and preferential source areas on global dust aerosol: results from a model study. J. Geophys. Res. Atmos. 107 (D21). https://doi.org/10.1029/2001jd000963.
Ternon, E., Guieu, C., Loÿe-Pilot, M.D., Leblond, N., Bosc, E., Gasser, B., Miquel, J.C., Martín, J., 2010. The impact of Saharan dust on the particulate export in the water column of the North Western Mediterranean Sea. Biogeosciences 7 (3), 809–826. https://doi.org/10.5194/bg-7-809-2010.
Theodosi, C., Parinos, C., Gogou, A., Kokotos, A., Stavrakakis, S., Lykousis, V., Hatzianestis, J., Mihalopoulos, N., 2013. Downward fluxes of elemental carbon, metals and polycyclic aromatic hydrocarbons in settling particles from the deep Ionian Sea (NESTOR site), Eastern Mediterranean. Biogeosciences 10 (7), 4449–4464. https://doi.org/10.5194/bg-10-4449-2013.
Theodosi, C., Markaki, Z., Pantazoglou, F., Tselepides, A., Mihalopoulos, N., 2019. Chemical composition of downward fluxes in the Cretan Sea (eastern Mediterranean) and possible link to atmospheric deposition: a 7 year survey. Deep-Sea Res. II Top. Stud. Oceanogr. 164, 89–99. https://doi.org/10.1016/j.dsr2.2019.06.003.
Tsagaraki, T.M., Herut, B., Rahav, E., Berman Frank, I.R., Tsiola, A., Tsapakis, M., Giannakourou, A., Gogou, A., Panagiotopoulos, C., Violaki, K., Psarra, S., Lagaria, A., Christou, E.D., Papageorgiou, N., Zervoudaki, S., Puelles, M.L.F.D., Nikolioudakis, N., Meador, T.B., Tanaka, T., Pitta, P., 2017. Atmospheric deposition effects on plankton communities in the eastern Mediterranean: a mesocosm experimental approach. Front. Mar. Sci. 4. https://doi.org/10.3389/fmars.2017.00210.
Tsagkaraki, M., Theodosi, C., Kanakidou, M., Mihalopoulos, N., 2020. Atmospheric deposition over the Aegean Sea and its impact on the seawater productivity. Springer International Publishing, pp. 207–227. https://doi.org/10.1007/698_2020_679.
Van Boxtel, A.P.E., Stuut, J.-B.W., Peterse, F., 2025. Identifying Saharan dust driven export of biogenic material in the ultraoligotrophic eastern Mediterranean Sea. Front. Mar. Sci. 12. https://doi.org/10.3389/fmars.2025.1537028.
Van der Does, M., Brummer, G.J.A., Van Crimpen, F.C.J., Korte, L.F., Mahowald, N.M., Merkel, U., Yu, H., Zuidema, P., Stuut, J.B.W., 2020. Tropical rains controlling deposition of Saharan dust across the North Atlantic Ocean. Geophys. Res. Lett. 47 (5). https://doi.org/10.1029/2019gl086867.
Van der Does, M., Knippertz, P., Zschenderlein, P., Giles Harrison, R., Stuut, J.-B.W., 2018. The mysterious long-range transport of giant mineral dust particles. Sci. Adv. 4 (12).
Van der Does, M., Korte, L.F., Munday, C.I., Brummer, G.J.A., Stuut, J.B.W., 2016. Particle size traces modern Saharan dust transport and deposition across the equatorial North Atlantic. Atmos. Chem. Phys. 16 (21), 13697–13710. https://doi.org/10.5194/acp-16-13697-2016.
Van der Does, M., Brummer, G.J.A., Korte, L.F., Stuut, J.B.W., 2021. Seasonality in Saharan dust across the Atlantic Ocean: from atmospheric transport to seafloor deposition. J. Geophys. Res. Atmos. 126 (11). https://doi.org/10.1029/2021jd034614.
Van der Jagt, H., Friese, C., Stuut, J.-B.W., Fischer, G., Iversen, M.H., 2018. The ballasting effect of Saharan dust deposition on aggregate dynamics and carbon export: aggregation, settling, and scavenging potential of marine snow. Limnol. Oceanogr. 63 (3), 1386–1394. https://doi.org/10.1002/lno.10779.
Van Hateren, J.A., Prins, M.A., Van Balen, R.T., 2018. On the genetically meaningful decomposition of grain-size distributions: a comparison of different end-member modelling algorithms. Sediment. Geol. 375, 49–71. https://doi.org/10.1016/j.sedgeo.2017.12.003.

Varga, G., Újvári, G., Kovács, J., 2014. Spatiotemporal patterns of Saharan dust outbreaks in the Mediterranean Basin. Aeolian Res. 15, 151–160. https://doi.org/10.1016/j.aeolia.2014.06.005.

Varkitzi, I., Psarra, S., Assimakopoulou, G., Pavlidou, A., Krasakopoulou, E., Velaoras, D., Papathanassiou, E., Pagou, K., 2020. Phytoplankton dynamics and bloom formation in the oligotrophic eastern Mediterranean: field studies in the Aegean, Levantine and Ionian seas. Deep-Sea Res. II Top. Stud. Oceanogr. 171, 104662. https://doi.org/10.1016/j.dsr2.2019.104662.

Vincent, J., Laurent, B., Losno, R., Bon Nguyen, E., Roullet, P., Sauvage, S., Chevaillier, S., Coddeville, P., Ouboulmane, N., Di Sarra, A.G., Tovar-Sánchez, A., Sferlazzo, D., Massanet, A., Triquet, S., Morales Baquero, R., Fornier, M., Coursier, C., Desboeufs, K., Dulac, F., Bergametti, G., 2016. Variability of mineral dust deposition in the western Mediterranean basin and south-east of France. Atmos. Chem. Phys. 16 (14), 8749–8766. https://doi.org/10.5194/acp-16-8749-2016.